The impact of the chemical production of methyl nitrate from the NO + CH 3 O 2 reaction on the global distributions of alkyl nitrates, nitrogen oxides and tropospheric ozone: a global modelling study

J.E. Williams, G Le Bras, Alexandre Kukui, H Ziereis, C. A. M. Brenninkmeijer

Atmos. Chem. Phys., 14, 2363–2382, 2014
www.atmos-chem-phys.net/14/2363/2014/
doi:10.5194/acp-14-2363-2014

Atmospheric Chemistry and Physics Open Access

The impact of the chemical production of methyl nitrate from the NO + CH_3O_2 reaction on the global distributions of alkyl nitrates, nitrogen oxides and tropospheric ozone: a global modelling study

J. E. Williams[1], **G. Le Bras**[2], **A. Kukui**[3], **H. Ziereis**[4], **and C. A. M. Brenninkmeijer**[5]

[1]Royal Netherlands Meteorological Institute, De Bilt, the Netherlands
[2]Institut de Combustion, Aérothermique, Réactivité et Environnement, CNRS, Orléans, France
[3]Laboratoire de Physique et Chimie de l'Environnement et de l'Espace, CNRS, Orléans, France
[4]DLR, Oberpfaffenhofen, Germany
[5]Max Planck Institute for Chemistry, Atmospheric Chemistry, Mainz, Germany

Correspondence to: J. E. Williams (williams@knmi.nl)

Received: 28 April 2013 – Published in Atmos. Chem. Phys. Discuss.: 2 August 2013
Revised: 9 December 2013 – Accepted: 9 January 2014 – Published: 7 March 2014

Abstract. The formation, abundance and distribution of organic nitrates are relevant for determining the production efficiency and resident mixing ratios of tropospheric ozone (O_3) on both regional and global scales. Here we investigate the effect of applying the recently measured direct chemical production of methyl nitrate (CH_3ONO_2) during NO_x recycling involving the methyl-peroxy radical on the global tropospheric distribution of CH_3ONO_2 and the perturbations introduced towards tropospheric NO_x and O_3 using the TM5 global chemistry transport model. By comparisons against numerous observations, we show that the global surface distribution of CH_3ONO_2 can be largely explained by introducing the chemical production mechanism using a branching ratio of 0.3 %, when assuming a direct oceanic emission source of $\sim 0.15\,\mathrm{Tg\,N\,yr^{-1}}$. On a global scale, the chemical production of CH_3ONO_2 converts $1\,\mathrm{Tg\,N\,yr^{-1}}$ from nitrogen oxide for this branching ratio. The resident mixing ratios of CH_3ONO_2 are found to be highly sensitive to the dry deposition velocity that is prescribed, where more than 50 % of the direct oceanic emission is lost near the source regions, thereby mitigating the subsequent effects due to long-range and convective transport out of the source region. For the higher alkyl nitrates ($RONO_2$) we find improvements in the simulated distribution near the surface in the tropics (10° S–10° N) when introducing direct oceanic emissions equal to $\sim 0.17\,\mathrm{Tg\,N\,yr^{-1}}$. In terms of the vertical profile of CH_3ONO_2, there are persistent overestimations in the free troposphere and underestimations in the upper troposphere across a wide range of latitudes and longitudes when compared against data from measurement campaigns. This suggests either a missing transport pathway or source/sink term, although measurements show significant variability in resident mixing ratios at high altitudes at global scale. For the vertical profile of $RONO_2$, TM5 performs better at tropical latitudes than at mid-latitudes, with similar features in the comparisons to those for CH_3ONO_2. Comparisons of CH_3ONO_2 with a wide range of surface measurements shows that further constraints are necessary regarding the variability in the deposition terms for different land surfaces in order to improve on the comparisons presented here. For total reactive nitrogen (NO_y) ~ 20 % originates from alkyl nitrates in the tropics and subtropics, where the introduction of both direct oceanic emissions and the chemical formation mechanism of CH_3ONO_2 only makes a ~ 5 % contribution to the total alkyl nitrate content in the upper troposphere when compared with aircraft observations. We find that the increases in tropospheric O_3 that occur due oxidation of CH_3ONO_2 originating from direct oceanic emission is negated when accounting for the chemical formation of CH_3ONO_2, meaning that the impact of such oceanic emissions on atmospheric lifetimes becomes marginal when a branching ratio of 0.3 % is adopted.

Published by Copernicus Publications on behalf of the European Geosciences Union.

1 Introduction

The chemical production of tropospheric ozone (O_3) is critically dependent on the recycling efficiency of NO to NO_2 involving peroxy radicals (Atkinson, 2000). The most abundant types of peroxy-radicals (RO_2) in the troposphere are the hydro peroxy (HO_2) and methyl peroxy (CH_3O_2) radicals, which are predominantly formed during the photolysis of chemical precursors such as formaldehyde (HCHO), and via oxidation of carbon monoxide (CO) and methane (CH_4) during recycling of OH radicals. Once formed in Reactions (R1)–(R3), NO_2 is rapidly photolysed, producing tropospheric ozone (O_3) by Reactions (R4) and (R5):

$$NO + HO_2 \rightarrow NO_2 + OH, \quad (R1)$$

$$NO + CH_3O_2(+O_2) \rightarrow NO_2 + HCHO + HO_2, \quad (R2)$$

$$NO + RO_2 \rightarrow NO_2 + RO, \quad (R3)$$

$$NO_2 + h\nu \rightarrow NO + O^3P, \quad (R4)$$

$$O^3P + O_2 + M \rightarrow O_3 + M. \quad (R5)$$

Loss of NO may also occur via the titration of O_3 (Reaction (6)), which moderates O_3 mixing ratios in high NO_x environments:

$$NO + O_3 \rightarrow NO_2 + O_2 \quad (R6)$$

On a global scale, Reaction (1) is the dominant NO_x recycling mechanism involving RO_2; it accounts for $\sim 65\,\%$ of total regeneration of NO_2, while Reactions (2) and (3) accounting for $\sim 25\,\%$ and $\sim 10\,\%$, respectively (see Sect. 5). However, Reaction (6) is the major NO-to-NO_2 recycling mechanism, where there is no net contribution towards the production of O_3 under steady state NO_x-O_3 conditions, meaning that it acts as a moderating step.

The chain length of the free-radical reaction cycle described above is determined by the efficiency of the chain termination steps in high NO_x environments, mainly Reactions (R7)–(R9) below. These lead to the formation of oxidised nitrogen reservoirs: nitric acid (HNO_3), peroxy-acetyl nitrate (PAN) and organic nitrates ($RONO_2$), respectively.

$$NO_2 + OH + M \rightarrow HNO_3 + M \quad (R7)$$

$$NO_2 + CH_3(O)O_2 + M \rightarrow PAN + M \quad (R8)$$

$$NO + RO_2 + M \rightarrow RONO_2 + M \quad (R9)$$

Although the individual steps of this reaction cycle have been studied extensively over the last decades, there is still some uncertainty related to the possibility of long lived nitrogen reservoirs being formed directly during Reactions (1) and (2). For instance, recent laboratory measurements using chemical ionisation mass spectroscopy have revealed the direct formation of HNO_3 from Reaction (1), where the branching ratio depends on pressure, temperature and relative humidity (Butkovskaya et al., 2005, 2007). This has led to a number of different global modelling studies associated with studying the impact of this branching ratio on tropospheric composition (Cariolle et al., 2009; Sovde et al., 2011; Gottschaldt et al., 2013; Boxe et al., 2012). The subsequent reduction in the recycling efficiency of NO reduces the production of tropospheric O_3, which lowers oxidative capacity. However, some ambiguity still exists as to the catalytic effects of water vapour on the branching ratio (Butkovskaya et al., 2009) meaning that the direct formation of HNO_3 is typically not included in chemical mechanisms employed in large-scale chemistry transport models (CTMs) nor currently included in the recommendations (e.g. Sander et al., 2011) due to the lack of an independent measurement for this branching ratio.

Using the same technique, Butkovskaya et al. (2012) recently detected the direct formation of methyl nitrate (CH_3ONO_2) from Reaction (2). The branching ratio (Reaction 10) inferred for tropospheric conditions is $1.0 \pm 0.7\,\%$, and it has a weak temperature and pressure dependence:

$$NO + CH_3O_2 + M \rightarrow CH_3ONO_2 + M. \quad (R10)$$

Results from a recent conceptual modelling study by Farmer et al. (2011) have suggested that the formation of $RONO_2$ during the conversion of NO to NO_2 by RO_2 under urban conditions has the potential to significantly reduce the photochemical production of O_3. Moreover, $RONO_2$ has also been found to be important for the lifetime of NO_x whenever the total NO_x mixing ratio is lower than 500 ppt (Browne and Cohen, 2012). Therefore, given the importance of Reaction (2) in the remote tropical troposphere in terms of NO_x recycling, where the largest amount of CH_4 is oxidised (Fiore et al., 2006), Reaction (10) could have implications for the global tropospheric O_3 burden. The formation of CH_3ONO_2 from the sequestration of NO_2 by the CH_3O radical has been invoked as another possible source, but it was considered insignificant on a global scale because of the high NO_2 mixing ratios which are necessary (Flocke et al., 1998a). The formation of CH_3ONO_2 during the decomposition of PAN was also suggested, although this mechanism was later shown to be rather inefficient (Orlando et al., 1992) and therefore is not included in this study.

Alkyl nitrates contribute significantly to the total reactive nitrogen (NO_y) budget of the troposphere (e.g. Buhr et al., 1990) but measuring them remains difficult. Nonetheless they have been measured under a wide range of atmospheric conditions (e.g. Flocke et al., 1998a, b; Blake et al., 1999; Swanson et al., 2003; Jones et al., 2011) typically by analysing flask measurements, although in some instances techniques such as gas chromatography with electron capture (Roberts et al., 1998), gas chromatography/mass spectroscopy (GC–MS; e.g. Dahl et al., 2005) and thermal dissociation/laser-induced fluorescence (TD–LIF; e.g.

Table 1. (a) Mixing ratios of CH_3ONO_2 measured at the surface over the last few decades. (b) The range of CH_3ONO_2 mixing ratios measured in the FT (between 2 and 10 km) during research flights over the last few decades from various measurement campaigns.

Region	Latitude	Lat./Long.	Mixing ratios (ppt)	Reference
(a)				
NH	73° N	38° W	∼ 4	Swanson et al. (2003)
	44° N	66° W	∼ 2	Roberts et al. (1998)
Tropics	20° N	156° W	∼ 4	Walega et al. (1992)
	0–17° N	150° E–150° W	2–50	Dahl et al. (2005)
	18° S–30° N	50° W–5° E	4–40	Chuck et al. (2002)
	16–24° S	133–145° E	∼ 5	Simpson et al. (2002)
SH	70° S	8° W	8–10	Weller et al. (2002)
	75.4° S	26.4° W	2–14	Jones et al. (2011)
	88–90° S	ALL	∼ 3–11	Swanson et al. (2004)
	88-90° S	ALL	∼ 4–13	Beyersdorf et al. (2010)
(b)				
NH	40–85° N	60–110° W	∼ 2–4	Blake et al. (2003b)
	30–40° N	20–40° W	∼ 2–3	Reeves et al. (2007)
Tropics/mid-lat.	2° S–60° N	115–155° W	∼ 3–4	Flocke et al. (1998a)
	40° S–40° N	150° E–140° W	1–27	Blake et al. (2003a)
Global	60° S–80° N	160° E–150° W	∼ 3–40	Blake et al. (1999)

Farmer and Cohen, 2008) have been used at the measurement location. In Tables 1a and b, we provide an overview of mixing ratios of CH_3ONO_2 which have been measured at both the surface and in the free troposphere (FT, between 2–10 km), respectively, where values are grouped in latitudinal zones. Although a large fraction of alkyl nitrates are formed in the gas phase via Reaction (9), other direct sources are thought to exist from direct oceanic emissions (Atlas et al., 1993; Chuck et al., 2002; Dahl et al., 2005) and, to a lesser extent, biomass and savannah burning (Simpson et al., 2002). Measurements of alkyl nitrates made over the tropical ocean, along with concentration gradients of dissolved $RONO_2$ measured in seawater surface, infer aqueous phase production until supersaturation occurs, followed by a release into the Marine Boundary Layer (MBL), with a dependency on the dissolved nitrite concentrations (Dahl and Saltzman, 2008). Such oceanic emissions act as a direct source of additional nitrogen reservoirs into low NO_x environments without the need of long-range transport. This biogenic source is likely to exhibit a latitudinal gradient related to the temperature of the surface waters and biological activity (Chuck et al., 2002; Dahl et al., 2007). For instance, measurements made at coastal sites in the US have found that direct emission from the ocean waters only makes a minor contribution to resident mixing ratios of CH_3ONO_2 near the east coast (Russo et al., 2010). Measurements on the Antarctic around 70–75° S have revealed surprisingly high resident mixing ratios of between 2–14 ppt CH_3ONO_2, indicating a possible link to NO_x emissions from snow (e.g. Weller et al., 2002; Wang et al., 2007). Compared to other alkyl nitrates, CH_3ONO_2 is the most abundant at these southerly latitudes (Jones et al., 2011). Similar measurements at the South Pole show a maximum of C1–C3 alkyl nitrates during austral wintertime (Beyersdorf et al., 2010). Here the authors propose the source not to be direct emissions from the snowpack, but rather transport from oceanic regions. However, there is little vertical structure in the regional profiles shown, meaning that any oceanic source would have to be rather weak. Therefore, the actual source of CH_3ONO_2 at these southerly latitudes is still the subject of some debate.

To investigate the global impacts on atmospheric composition, Neu et al. (2008) used a CTM to show that biogenic alkyl nitrates exert an impact on the tropospheric O_3 and NO_x budgets in the tropics. In their study they adopted a priori emission estimates based on the measurements presented in Blake et al. (2003a) for both CH_3ONO_2 and ethyl nitrate ($C_2H_5ONO_2$). However, the chemical formation of CH_3ONO_2 via Reaction (10) was not considered. Including Reaction (10) could go some way to accounting for the observed resident mixing ratios in the remote marine troposphere, on Antarctica and in the FT (Blake et al., 2003a; Walega et al., 1992; Flocke et al., 1998a). This would result in a lower emission flux estimate being needed to explain ambient air measurements. Once present, alkyl nitrates are removed by either deposition processes (e.g. Russo et al., 2010), direct photolytic dissociation, or oxidation by OH (Talukdar et al., 1997a, b) to release NO_2. Thus the potential reduction in the production efficiency of tropospheric O_3 by Reaction (2) due to Reaction (10) has the potential to neutralise the effects of increased oceanic nitrogen emissions.

In this paper we investigate the global impact that the proposed chemical formation of CH_3ONO_2 has on composition

of the global troposphere by using the tropospheric version of the global 3-D Chemistry Transport Model (CTM) TM5. In Sect. 2 we provide a description of the version of TM5 used for the study, the emission estimates adopted for precursor trace gases, and the updates made compared to previous model versions and details of the inclusion of CH_3ONO_2. In Sect. 3 we examine the distribution of both CH_3ONO_2 and higher alkyl nitrates in TM5 after including both the direct oceanic emission sources and the chemical production from Reaction (10). We also examine how the introduction of extra nitrogen into the troposphere alters the reactive nitrogen budget. In Sect. 4 we compare the distribution of alkyl nitrates at high latitudes and in the tropics against those measured during a number of intensive campaigns, and we identify the sensitivity of the vertical and regional distribution towards assumptions in both emissions and chemical formation. In Sect. 5 we show the effects on tropospheric NO_x, O_3 and OH and discuss implications for the atmospheric lifetimes of greenhouse gases. Finally, in Sect. 6, we present our conclusions.

2 Model description

2.1 The TM5 model

In this study we use the 3-D global CTM TM5 (Huijnen et al., 2010; Williams et al., 2013) which employs the modified CB05 chemical scheme. This mechanism has recently been comprehensively described and validated in Williams et al. (2013) so for brevity we do not provide many details here. We perform simulations at a horizontal resolution of $3^\circ \times 2^\circ$ and use 34 vertical levels from the surface up to ~ 0.5 hPa. TM5 is driven using meteorological fields taken from the ERA-interim re-analysis (Dee et al., 2011), using an update frequency of 3 h. The details of which parameters from the meteorological fields are used in TM5 are given in Huijnen et al. (2010). The chosen simulation year is 2008 and all simulations use 2007 as a one-year spin-up period to reach chemical equilibrium.

Some modifications which improve TM5 compared to previous versions have also been incorporated (e.g. Williams et al., 2013) as described here. As this version of TM5 only contains tropospheric chemistry, observational constraints are applied in the stratosphere for species such as CH_4 and O_3 (Huijnen et al., 2010). We also adopt new boundary conditions for HNO_3 based on the HNO_3 / O_3 ratios derived using latitudinal climatologies assembled from measurements by the ODIN instrument between 2001 and 2009 (Jégou et al., 2008; Urban et al., 2009), where instantaneous forcing is applied at 10 hPa. This provides a more realistic seasonal evolution of HNO_3 in the stratosphere when compared to that simulated when using the Upper Atmosphere Research Satellite (UARS) climatology in previous versions (Huijnen et al., 2010; Williams et al., 2012), especially in the polar regions. Previous studies have shown that the global dry deposition flux of carbon monoxide (CO) in TM5 was rather high, accounting for the loss of 160–180 Tg CO yr^{-1} (e.g. Williams et al., 2012). In this study the loss of CO at the surface by enzymatic processes in the soil (Yonemura et al., 2000) is parameterised with respect to the soil moisture content according to Sanderson et al. (2003). The resistive fluxes are then passed into the dry deposition scheme of Ganzeveld and Lelieveld (1995). This reduces the global dry deposition flux by around ~ 80 Tg CO yr^{-1}. Further updates associated with dry deposition include increasing the surface resistance for CO over oceans and of O_3 over snow and ice. Finally we improved the carbon balance in the CH_3O_2 self-termination reaction by adopting the CB05 reaction nomenclature given in Yarwood et al. (2005).

For this study we have included CH_3ONO_2 explicitly as an additional transported tracer species. The atmospheric lifetime of CH_3ONO_2 is estimated to range from around a week to a month depending on atmospheric conditions (Talukdar et al., 1997a, b), meaning that it can be transported out of the Boundary Layer (BL; the first few kilometres near the surface) into the FT and beyond. This is compared to atmospheric lifetimes of between several days to weeks for the C2–C5 $RONO_2$ (Clemitshaw et al., 1997). Both the photolytic destruction and oxidation of CH_3ONO_2 by OH are included using the chemical reaction data taken from Talukdar et al. (1997a, b) forming the products NO_2 and HCHO. We also include a dry deposition term equal to that used for the C2–C4 $RONO_2$ for the majority of the simulations. A small wet deposition term is also included, using the values of Kames and Schurath (1992).

2.2 Definition of the emission scenarios and sensitivity studies

The emission estimates used here are described in Williams et al. (2013), and are thus only briefly summarised here. For anthropogenic emissions we use a hybrid complied using the RETRO inventory (Schultz et al., 2007; http://retro.enes.org) and the REAS (Regional Emission Inventory in Asia) inventory for the Asian region (Ohara et al., 2007) between 60–150° E and 10° S–50° N. The exception is CH_4, which we take from EDGARv4.2 (http://edgar.jrc.ec.europa.eu/). For biomass-burning emissions, we use the GFEDv3 monthly emission inventory (van der Werf et al., 2010). For biogenic emissions we use the estimates provided by MEGANv2 (Guenther et al., 2006) except for CH_4, which we take from the LPJ-WHyMe (LPJ-Wetland Hydrology and Methane) inventory (Spahni et al., 2011). For lightning NO_x we use the parameterisation of Meijer et al. (2001). The CH_4 distribution in the boundary layer is constrained by nudging to a seasonally dependant latitudinal gradient up to 500 hPa using the method given in Williams et al. (2013).

In total, six sensitivity studies are defined and listed in Table 2, in addition to the BASE simulation which does

Table 2. An overview of the sensitivity studies performed with TM5 to investigate the impact of the chemical production of CH_3ONO_2 on global tropospheric composition.

Model simulation	Direct oceanic emissions	Branching ratio	Comments
BASE	NO	N/A	Default modified CB05 chemistry without CH_3ONO_2 and no oceanic emissions
EMISS	YES	N/A	Adopting the emission estimates for CH_3ONO_2 from Neu et al. (2008) between 10° S and 10° N
DEMISS	YES	N/A	Adopting an emission twice that of Neu et al. (2008) between 10° S–10° N
LOWBR	NO	0.3 %	Lower uncertainty range from Butkovskaya et al. (2012)
HIGHBR	NO	1.0 %	Branching ratio measured by Butkovskaya et al. (2012)
FULL	YES	0.3 %	Combined emissions (0.5 of EMISS) and direct production (as in LOWBR)
DDEP	YES	0.3 %	As FULL, except the dry deposition flux is increased by 100 %
FLIGHT	YES	0.025 %	As DEMISS, except adopting the branching ratio suggested in Flocke et al. (2003a) derived from measurements

not explicitly include CH_3ONO_2. These are, namely, (1) EMISS, which applies a direct a priori oceanic emission for CH_3ONO_2 of 26.7 $mg\,m^{-2}\,s^{-1}$ ($\sim 0.29\,Tg\,yr^{-1}$) as taken from Neu et al. (2008) and applied between 10° S-10° N; (2) DEMISS, which applies a direct a priori oceanic emission flux for CH_3ONO_2 twice that of EMISS to represent an upper limit; (3) LOWBR, with which we adopt a low branching ratio of 0.3 % for the chemical formation of CH_3ONO_2 (the lower limit of the experimental data in Butkovskaya et al., 2012); (4) HIGHBR with a branching ratio of 1.0 %; (5) FULL, with which we reduce the direct emission by 50 % compared to EMISS and apply the low branching ratio of 0.3 %; (6) DDEP, applied in the same manner as FULL, except we double the dry deposition flux of CH_3ONO_2; and (6) FLIGHT, applied in the same manner as DEMISS, except that we use a branching ratio of 0.025 % which is the mean value suggested by Flocke et al. (1998a) derived from measurements made in the upper troposphere (UT; above 10 km until the tropopause). In the EMISS, FULL, DDEP and FLIGHT simulations we also include the direct emissions of $RONO_2$ from the ocean, adopting an estimate of 15.62 $mg\,m^{-2}\,s^{-1}$ ($\sim 0.17\,Tg\,N\,yr^{-1}$), which is twice the a priori estimate calculated for $C_2H_5ONO_2$ in Neu et al. (2008) so as to represent the release of other alkyl nitrates such as e.g. isopropyl nitrate as measured over the tropical ocean (Dahl et al., 2005). Direct emissions of alkyl nitrates from the oceans are applied out away from coastlines by using the land–sea mask threshold of 15 % in each grid cell to exclude large freshwater lakes and landlocked bodies of water in the tropics. In our study – unlike in Neu et al. (2008), which was motivated by the measurements of Blake et al. (2003a) – no oceanic emissions are applied in the SH. The emission of alkyl nitrates from the ocean has been linked to both the concentration of chlorophyll and sea temperature (Chuck et al., 2002; Dahl and Saltzman, 2008). A strong seasonality exists in the chlorophyll concentrations in the SH (Myriokefalitakis et al., 2010) resulting in maximal concentrations occurring during the boreal wintertime; therefore any resulting emission flux is likely to exhibit a similar seasonality. The small emission of CH_3ONO_2 measured from biomass and savannah fires ($\sim 18\,Gg\,yr^{-1}$, Simpson et al., 2002) is an order of magnitude lower than the ocean emission flux and thus is not included.

2.3 Observational data sets

To investigate to what degree TM5 is able to capture a realistic global distribution of alkyl nitrates on global scale we compare model output co-located with independent measurements made at selected stations and by research aircraft. Relevant details on these sites and campaigns are given in the following.

The Halley Bay research station at coastal Antarctica (75.3° S, 26.4° W) is situated 32 m above sea level and located on the Brunt Ice shelf. It is surrounded on three sides by the Weddell Sea and can be near ice-free water during the austral summer months. For our study we use the measurements presented in Jones et al. (2011) taken as part of the Chemistry of the Antarctic Boundary Layer and the Interface with Snow (CHABLIS) campaign which took place from February 2004 to January 2005. Measurements were performed on samples stored in flasks which were transported and analysed in the United Kingdom by gas chromatography–mass spectroscopy.

Neumayer, in Antarctica (70.0° S, 8.2° W), is a well-established measurement station. It is located on an ice shelf ∼ 10 km away from the northeastern Weddell Sea, and is considered to be representative of a location with pristine air transported either over the snow pack on Antarctica or from over the surrounding ocean and sea ice. Here we use the measurement values published by Weller et al. (2002), who analysed air from flasks by gas chromatography to determine mixing ratios of alkyl nitrates.

The Mauna Loa Observatory is located ∼ 3.4 km above sea level in Hawaii (19.5° N, 155.6° W), which is situated in the remote northern Pacific Ocean. It has a long-standing history of measuring atmospheric composition, and we use values observed during the Mauna Loa Observatory Photochemistry Experiment (MLOPEX, Ridley and Robinson, 1992). These measurements are representative of FT air and therefore should provide information regarding background mixing ratios. Again, the measured values published in Walega et al. (1992) are derived using gas chromatography with a detection limit of ∼ 0.3 ppt for $RONO_2$.

For the extratropical NH we use the values provided in Roberts et al. (1998) measured at Chebogue Point, Nova Scotia (43.8° N, 66.1° W) as part of the North Atlantic Regional Experiment (NARE; Fehsenfeld et al., 1996) during August and September 1993. The measurement site is located at the tip of a peninsula about 10 km south of Yarmouth, Nova Scotia. The location was chosen such that strong anthropogenic NO_x sources towards the south did not impinge significantly on the measurements, although there was some local ship traffic (Fehsenfeld et al., 1996). Therefore, these measurements are thought to be representative of the remote conditions affected by oceanic air masses.

To assess the vertical distribution of CH_3ONO_2 and $RONO_2$ in the TM5 model at tropical latitudes, we use data obtained during a number of different flights conducted as part of the second Pacific Exploratory Mission (PEM-Tropics B; Raper et al., 2001) between March and April 1999 in the region 76° E–148° W and 36° S–38° N. Measurement data from both the DC-8 and P-3B aircraft have been used, which use different instrumentation for measuring the mixing ratios. For the comparison we interpolate three-hourly model data to the altitude and location at which the measurements were taken. The measurement data are averaged approximately every minute to avoid fluctuations in mixing ratios due to small-scale variability. These measurements have been presented in Blake et al. (2003a) and provide valuable information regarding the tropospheric distribution of these important NO_x reservoirs.

For the high northern latitudes we use measurements made during the Arctic Research of the Composition of the Troposphere from Aircraft and Satellites (ARCTAS) mission, which took place during two separate phases during April and June/July 2008 (Jacob et al., 2010). Only data from the DC-8 aircraft are used, which was based at Fairbanks (65° N, 148° W), Alaska during April and Cold Lake (54° N, 110° W), Alberta, Canada during June/July. As well as capturing some seasonality for the region, these measurements cover a large range of northern latitudes between 50–70° N across a wide longitudinal range, where the details of exact locations are given in Jacob et al. (2010). For our comparisons we use the same averaging technique to that utilised for the PEM-tropics B data, where the measurement data is again averaged approximately every minute. To our knowledge this is the first time that this alkyl nitrates data has been used in a global model study.

Finally, we use chemical NO_y measurements from the second phase of the Civil Aircraft for Regular Investigation of the Atmosphere Based on an Instrument Container (CARIBIC) project, which started in 2005 and continues to run (Brenninkmeijer et al., 2007). In this instance NO_y is defined as the cumulative sum of all reactive nitrogen species, namely NO, NO_2, PAN, HNO_3, HNO_4, N_2O_5 and all alkyl nitrates. All trace constituents are reduced to NO during the measurement, meaning that no values are available for individual reservoir species. We use in situ measurements made from April until December 2008 made during flights from Frankfurt, Germany (50.0° N, 8.5° E) to Chennai, India (13.0° N, 80.2° E). The flights to and from Chennai take similar routes to those shown in Schuck et al. (2010), providing a monthly snapshot of the distribution of NO_y at the cruise altitude of 10–12 km throughout a large fraction of the year. The uncertainty associated with the CARIBIC NO_y measurements is ∼ 8 % for mixing ratios around 450 ppt. We only use measurements which are representative of the upper troposphere (UT), which restricts us to the latitude range 15–30° N.

3 The annual mean distribution of CH_3ONO_2 and $RONO_2$

Figure 1 shows both the annual zonal and horizontal mean distributions of CH_3ONO_2 for EMISS, along with the corresponding absolute differences in mixing ratios relative to FULL given in ppt, thus differentiating the impact of Reaction (10). For the annual horizontal mean distribution, mixing ratios are averaged between the surface and 800 hPa so as to give a representative value of the first few kilometres of

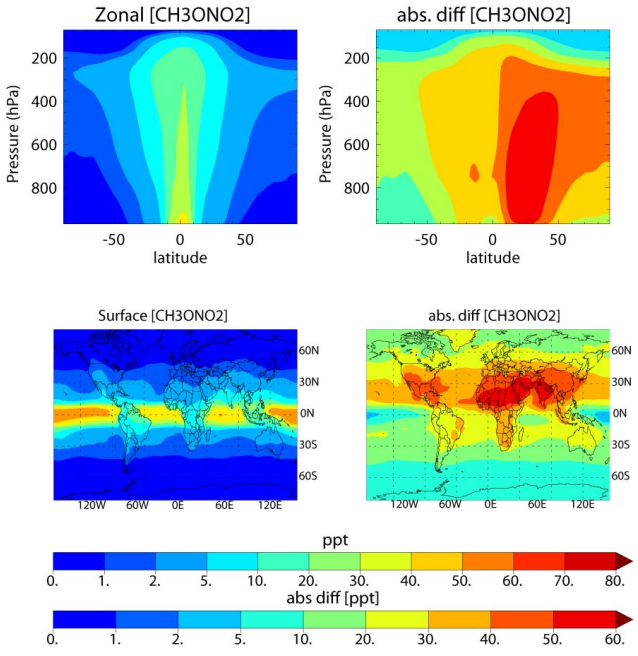

Fig. 1. The annual mean distribution in CH_3ONO_2 during 2008. Both the zonal and horizontal means are shown (top and bottom, respectively) for EMISS. The right panels show the absolute differences for FULL-EMISS given in ppt.

the troposphere. The total cumulative emission of CH_3ONO_2 in EMISS is equivalent to $\sim 0.3\,\mathrm{Tg\,N\,yr^{-1}}$ and results in a global tropospheric burden of 0.015 Tg N. The highest mixing ratios of between 40–60 ppt occur in the tropical MBL directly above the emission sources, where CH_3ONO_2 is lifted out of the MBL reaching the UT. Long-range transport towards higher latitudes then occurs by the large-scale atmospheric circulation. Unlike the vertical distribution shown in Neu et al. (2008), which exhibits maximal mixing ratios both in the BL and higher up in the UT, we do not get any increases in mixing ratios above 10 km in EMISS, but rather a continuous decrease as determined by the increasing efficiency of photolytic destruction with altitude and that the only source in EMISS is emission at the surface. We also do not have high mixing ratios in the SH as we only introduce oceanic emissions in the tropics, since the location of oceanic emissions is constrained by observations made by ships (e.g. Dahl et al., 2005). One complication is that there appears to be a large variability in the vertical profile of CH_3ONO_2 at similar latitudes from the available measurements when comparing campaigns. For instance, the measurements of Flocke et al. (1998a) indicate that the mixing ratio of CH_3ONO_2 should be between 1–3 ppt around 11km at tropical latitudes, which almost matches the zonal mean values shown for EMISS in Fig. 1. However, the profiles shown in Blake et al. (2003a) show higher mixing ratios in the tropical UT towards the Pacific (of between 10–15 ppt). This implies that there is a significant longitudinal variability in emission sources as determined by differences in biogenic activity. The long-range transport of CH_3ONO_2 out of the tropics below 800 hPa at higher latitudes is shown to be negligible due to loss by deposition at the surface. The global tropospheric lifetime of CH_3ONO_2 in EMISS is ~ 20 days, well within the estimates of between 7 days to a month as given in the literature (Butkovskaya et al., 2012). Chemical destruction predominantly occurs in the tropics, where dry deposition accounts for $\sim 50\,\%$ of the total sink term. However, in these simulations we did not employ a specific deposition flux for CH_3ONO_2, but used that of $RONO_2$ – which is assumed to be equal to the deposition flux of PAN – as a proxy (Huijnen et al., 2010). Comparing these solubility parameters to those given in Sander (1999) shows that this estimate is potentially too high by $\sim 25\,\%$. However for CH_3ONO_2, Russo et al. (2010) needed to increase the deposition velocity to values similar to that of O_3 in order to fit measured diurnal profiles. This motivated us to perform the DDEP simulation using enhanced deposition rates, which is discussed later on.

When introducing Reaction (10), absolute differences of between 20–60 ppt occur in the mean CH_3ONO_2 mixing ratios. The largest increases are situated over continental regions in the NH around the subtropics and tropics in the FT, above where most surface NO_x is emitted. It should be noted that these increases occur in spite of the 50 % reduction in the direct oceanic emission term for CH_3ONO_2 in FULL, to account for the introduction of a mixed source (see Table 2). This reduces the direct emission of CH_3ONO_2 to $\sim 0.15\,\mathrm{Tg\,N\,yr^{-1}}$ in FULL. Table 3 provides an annual tropospheric chemical budget for EMISS and FULL, along with that for other selected simulations. The troposphere is defined as the 150 ppb monthly mean contour in tropospheric O_3, as described in Stevenson et al. (2006). Comparing terms given in Table 3 shows that the direct emission of CH_3ONO_2 applied in FULL is smaller than the total formed in Reaction (10) by approximately a factor of seven. The global tropospheric burden of CH_3ONO_2 in FULL increases significantly, to ~ 0.08 Tg N ($\sim$ more than six times that found in EMISS). This increases the resulting global CH_3ONO_2 lifetime to 25.3 days, this time with chemical destruction being the dominant loss term ($\sim 55\,\%$) due to a smaller fraction of CH_3ONO_2 being near the surface.

When analysing the horizontal distribution of the absolute changes in the mixing ratios in Fig. 1 it follows that the highest differences are situated in the NH between 10–30° N over northern Africa, the Middle East and India. Part of this variability can be related to the regional differences in the deposition terms for CH_3ONO_2 as shown in Fig. 2. Here the regional variability in annual deposition terms from FULL is given, where the integrated annual deposition varies by an order of magnitude depending on surface type and local mixing ratios. The highest annual deposition occurs over the tropical oceans near regions close to where direct oceanic emissions are prescribed. The lowest deposition occurs over

Table 3. The annual tropospheric chemical budget terms for CH_3ONO_2 for 2008 given in Tg N yr^{-1} for selected simulations.

	EMISS	DEMISS	LOWBR	FULL	FLIGHT
Emission	0.286	0.573	0.000	0.142	0.573
$NO + CH_3O_2$	N/A	N/A	0 .990	0.994	0.084
$OH + CH_3ONO_2$	0.011	0.023	0.047	0.053	0.027
$CH_3ONO_2 + h\nu$	0.124	0.248	0.476	0.540	0.289
Dry deposition	0.139	0.279	0.429	0.500	0.317
Wet deposition	0.008	0.017	0.006	0.017	0.020

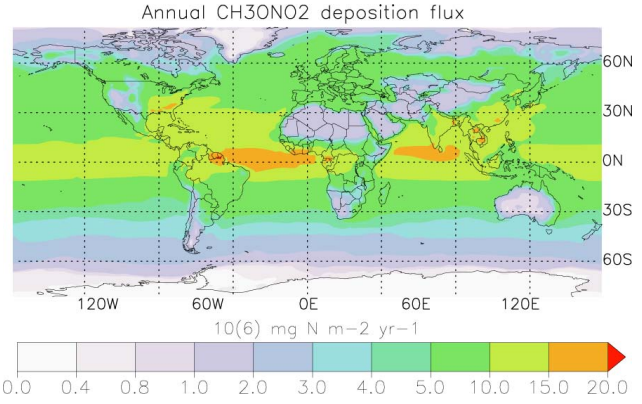

Fig. 2. The annually integrated global deposition flux of CH_3ONO_2 during 2008 from FULL. The values are given in 10^6 mg N m^{-2} yr^{-1}.

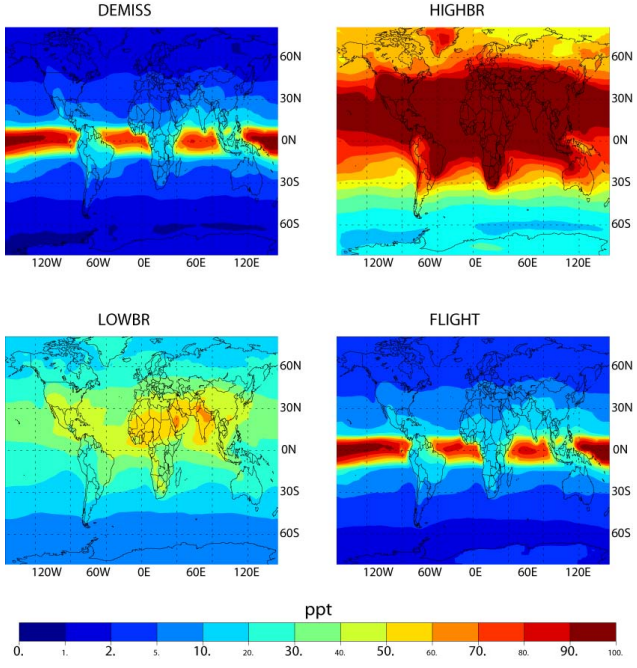

Fig. 3. The annual mean near surface distribution of CH_3ONO_2 during 2008 for **(a)** DEMISS, **(b)** HIGHBR **(c)** LOWBR and **(d)** FLIGHT given in ppt.

arid regions such as the Sahara and Antarctica. Examining the chemical budget terms shows that approximately half of the CH_3ONO_2 released from tropical emissions is lost by local deposition. This rapid turnover highlights the importance of placing constraints on deposition velocities by measurements, especially over the ocean, whose surface area in the tropics exceeds that of the continents. Such information would help the modelling community in being able to gauge the ability of atmospheric models to capture this important physical sink process. For the fraction of CH_3ONO_2 oxidised, photolytic destruction accounts for > 90 % of the total loss term. When comparing the chemical budget terms between EMISS and FULL it can be seen that Reaction (10) significantly reduces the contribution of direct oceanic emissions of CH_3ONO_2 to the global nitrogen budget. We discuss the implications for tropospheric O_3 production and oxidative capacity later on in Sect. 5.

To highlight the variability which is introduced across simulations with respect to the distribution of CH_3ONO_2, Fig. 3 shows the annual horizontal mean distribution of CH_3ONO_2 for DEMISS, HIGHBR, LOWBR and FLIGHT, respectively, again avergaed between the surface and 800 hPa. Table 3 provides the corresponding annual chemical budget terms for the majority of these simulations, allowing for the comparison of source and sink terms. Comparing the fractional loss due to deposition in Table 3 for EMISS and DEMISS shows that when restricting the source of CH_3ONO_2 to surface emissions, the amount lost by deposition scales rather linearly with the prescribed oceanic emission flux. Thus, the impact of direct emissions of CH_3ONO_2 is much less than from other sources of NO_x such as lightning or aircraft emissions, which occur in the FT due to the mitigation introduced by deposition. Figure 3 shows that the chemical production is most efficient where the chemical precursors have the highest mixing ratios, i.e. between 30° S and 40° N (not shown). Comparing the surface distribution of CH_3ONO_2 in HIGHBR and values presented in Table 1b from surface measurements shows that using a 1 % branching ratio overestimates observed values by an order of magnitude, and for

Table 4. The annual tropospheric chemical budget terms for $RONO_2$ for 2008 as calculated in the modified CB05 chemical mechanism as given in $Tg\,N\,yr^{-1}$ for selected TM5 simulations. The term for total nitrogen deposition is defined as the sum of dry and wet deposition of NO_2, HNO_3, $RONO_2$ and PAN.

	BASE	FULL
Emission	N/A	0.168
$NO + XO_2N$	11.205	11.197
$NO_3 + C_3H_6$	0.056	0.056
$NO_3 + ISOP$	2.317	2.311
$NO_3 + TERP$	1.010	1.008
$OH + RONO_2$	1.289	1.313
$RONO_2 + h\nu$	4.489	4.581
Dry deposition	2.874	2.940
Wet deposition	6.225	6.343
Global burden	0.173	0.176
Total N deposition	48.390	48.541

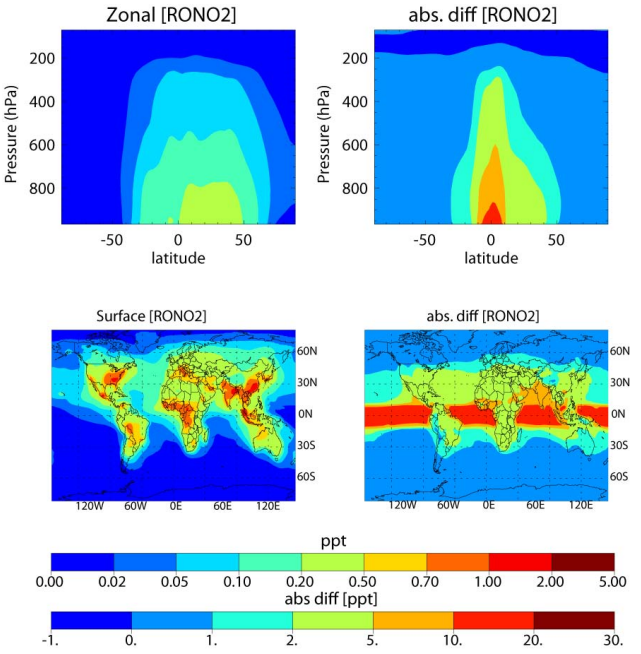

Fig. 4. The annual global distribution in $RONO_2$ during 2008 given in ppb. Both the zonal and horizontal (< 800 hPa) means are shown (top and bottom, respectively) for the BASE simulation. The absolute differences when compared against the FULL simulation are also given, with differences being in the ppt range.

this reason, this simulation is not discussed further here. For LOWBR, mixing ratios between 20–70 ppt occur between 30° S–30° N, where maximal mixing ratios occur over terrain with low deposition velocities (cf. Fig. 2). There is also an amplification of a few percent in the total chemical production term as a consequence of introducing oceanic emissions, although this is a rather weak feedback linked to enhancements in oxidative capacity (and thus CH_3O_2).

Figure 4 shows the corresponding global distribution of $RONO_2$ in BASE and Table 4 provides the corresponding global chemical budget terms for $RONO_2$ in both the BASE and FULL. The absolute differences between these simulations in mean mixing ratios for $RONO_2$ are also shown. Analysing the chemical budget for BASE reveals that in the modified CB05 mechanism, $RONO_2$ is predominantly formed via the conversion of NO with the NO_x operator species XO2N (Gery et al., 1989) and the oxidation of isoprene with the nitrate radical during nighttime. Figure 4 shows that the highest mixing ratios occur in regions where both anthropogenic and biogenic emissions dominate (e.g. eastern Asia and over Amazonia). Analysing the annual zonal mean shows that in the FT mixing ratios are higher in the NH. Introducing direct oceanic emissions increases the resident mixing ratios by $\sim 100\,\%$ at the surface and between ~ 5–$20\,\%$ in the FT. When examining the absolute differences in $RONO_2$ shown in Fig. 4, one can see that the largest occur in the tropics directly over the emission source regions. As for CH_3ONO_2, the chemical production term dominates over the direct emission. The global tropospheric burden of $RONO_2$ in the FULL simulation is 0.18 Tg N, giving a global tropospheric lifetime of 4.2 days, shorter than the value given for mid-latitudes in the literature by about a week (Clemitshaw et al., 1997). This is possibly due to 50 % being lost in the tropics and that adopting the deposition flux of PAN as a proxy results in too efficient loss by deposition, which exceeds that lost by chemical destruction. Finally, in Table 4 we also show the total summed N deposition terms for NO_2, HNO_3, PAN and $RONO_2$. Here N deposition increases by $\sim 0.15\,Tg\,N\,yr^{-1}$ (also for EMISS, not shown); thus ultimately the additional N introduced by direct emission is almost entirely lost via deposition.

4 Comparisons against surface and aircraft measurements

Over the last few decades there have been a number of measurement campaigns and initiatives on different scales that have observed CH_3ONO_2 mixing ratios at pristine locations and throughout the FT providing some information regarding background mixing ratios found in the troposphere. In Tables 1a and b we have summarised the resident mean mixing ratios of CH_3ONO_2 available in the literature from the last few decades, showing the vertical and latitudinal variability which exists on a global scale. For our purpose we subsequently select some of the surface sites, aircraft measurements at high northern latitudes and the measurements of Blake et al. (2003a, b) in the tropics to validate the global distribution of CH_3ONO_2 in TM5.

Figure 5 shows the daily variability in CH_3ONO_2 in the DEMISS, HIGHBR, FULL and DDEP simulations as calculated for Chebogue Point, Nova Scotia (44° N, 66° W), Mauna Loa, Hawaii (20° N, 156° W), Neumayer (70° S, 8° W) and Halley (75° S, 26° W) in Antarctica. We exclude EMISS as the transport to the measurement sites is negligible and therefore cannot explain the observed mixing ratios. For these comparisons, three-hourly model output is averaged into daily means in order to partially account for the impact of any diurnal cycle on resident mixing ratios due to photolytic destruction. The measurement data derived at these sites have been published in Roberts et al. (1998), Walagu et al. (1992), Weller et al. (2002) and Jones et al. (2011), respectively, although time-resolved measurements are not provided for Chebogue Point and therefore are not shown. The comparison clearly shows that HIGHBR results in an excess of CH_3ONO_2, with mixing ratios approximately an order of magnitude too high for the NH sites shown and a factor of two too high for Antarctica. Assuming that there is not an important sink process missing from the simulations, such as heterogeneous uptake into particles, these comparisons suggest that the lower limit of the branching ratio measured by Butkovskaya et al. (2012) seems the most plausible value.

At Chebogue Point (where a mean value of ~ 2 ppt has been observed in the summertime) the DEMISS simulation results in the best agreement due to the efficient loss during the long-range transport from the tropics. At a measurement site in the US, Russo et al. (2010) found that higher CH_3ONO_2 measurements correlated with continental air masses influenced by anthropogenic emissions and could not be explained by oceanic sources. However, FULL overestimates the resident mixing ratios by an order of magnitude, implying the need for a larger sink term or lower regional NO_x emissions from, e.g. soil. The dry deposition term has also been shown to be a crucial factor in being able to capture observed mixing ratios at surface sites on the east coast of the US (Russo et al., 2010). Comparing DDEP shows that there is some improvement, although the sink term rate at this site could still be too low. For instance, the ratio of the dry deposition flux against O_3 is ~ 0.6 compared with unity as suggested from the nighttime measurements of Russo et al. (2010). However, deposition velocities are related to the type of terrain meaning measurements on a local scale cannot be adopted on a global scale, which shows the necessity of more measurements related to the deposition fluxes of alkyl nitrates over various terrain types.

At Mauna Loa (mean value of 3.6 ± 1.8 ppt throughout May; Walega et al., 1992) the air is sampled in the remote FT and, thus, is affected by the long-range transport of CH_3ONO_2 from other source regions. DEMISS shows a signature of northerly transport from the tropics throughout the year, which overestimates mixing ratios by around ~ 5–10 ppt. For FULL, there is a large overestimation (of tens of ppt) in contrast to the comparisons against the PEM-tropics

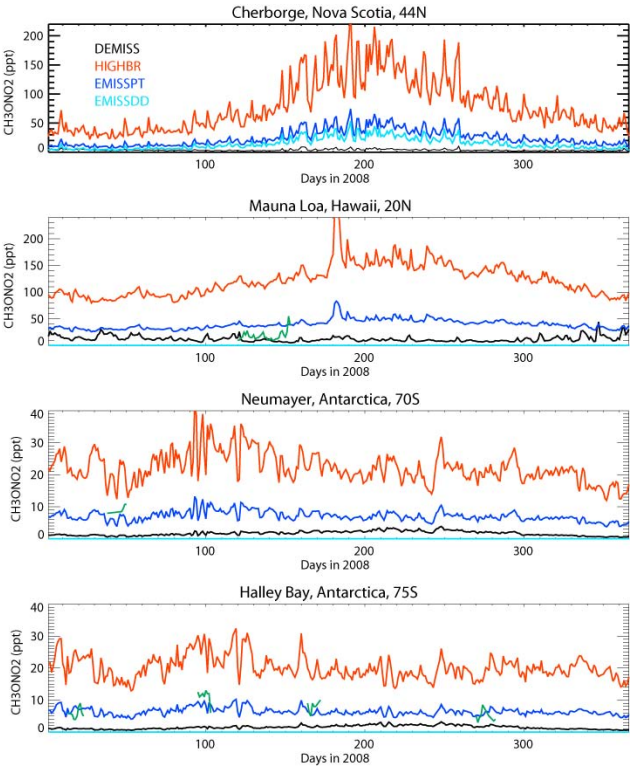

Fig. 5. Daily mean mixing ratios of CH_3ONO_2 in the DEMISS, HIGHBR, FULL and DDEP simulations extracted at Chebogue (45° N, top), Mauna Loa (20° N, upper middle), Neumayer (70° S, lower middle) and Halley Bay (75° S, bottom). Where available, the observed mixing ratios of CH_3ONO_2 are shown in green (see text for details). The simulations shown are EMISS (black), HIGHBR (red), FULL (dark blue) and DDEP (cyan).

data (see below) indicating there is likely a significant variability in the oceanic emission source term with respect to location. Conversely, DDEP underestimates observed mixing ratios as a result of doubling the deposition velocity over the ocean. Again, this shows the sensitivity of the simulations to the prescribed deposition fluxes. Mauna Loa is also affected by the long-range transport of CH_3ONO_2 from Asia, especially during spring (Jaffe et al., 1997). Such an increase can be seen around day 180 in both HIGHBR and FULL, but not for DEMISS, which is representative of northerly transport from pristine regions. Therefore, the measurement location is influenced by both local and remote sources.

At Neumayer and Halley (mean values of 8–10 ppt and 6–14 ppt, respectively), which are in relative close proximity, FULL provides the best agreement of all simulations, with DDEP being much too low. Comparing FULL and DEMISS shows that model mixing ratios above Antarctica are principally driven by Reaction (10) in our simulations. The signature of DEMISS becomes visible during the austral winter, where no photolytic destruction occurs and the deposition flux is lower due to extended sea-ice (see Fig. 2 for

differences in deposition fluxes with type of surface area). One missing potential source of trace species important for local CH_3ONO_2 production is the direct emission of NO_x, HCHO and hydrogen peroxide from the snowpack (Perrier et al., 2002; Wang et al., 2007; Thomas et al., 2012). Implementing such emission sources in TM5 could result in DDEP becoming the simulation with the best agreement, although current emission inventories for very high latitudes do not include such fluxes due to their high uncertainty. In the study of Neu et al. (2008) mixing ratios of between 35–40 ppt of CH_3ONO_2 occurred in the LT for latitudes below 60° S as a result of prescribing emissions in the SH, which are too high when compared to these measurements (see Tables 1a and b), similar to HIGHBR. Furthermore, the observed variability in CH_3ONO_2 at Neumayer did not show any correlation with the origin of air masses; this provides further evidence of the importance of some type of local source term such as a chemical production term investigated here (Weller et al., 2002).

Next we compare the tropical distribution of CH_3ONO_2 and $RONO_2$ in TM5 with those observed in the measurement data from the PEM-tropics B campaign during March 1999. The PEM-tropics B data is scaled up 2.13 times as instructed by the data providers (D. Blake, personal communication, 2013). The routes of the flights which are used in this study are presented in Fig. 6, with flights from the DC-8 and P-3B being shown as separate colours. It can be seen that measurements which occur over a wide area are used for our comparison. Although our simulation is for 2008 rather than 1999, the emissions employed are not dependent on, e.g. wind speed, chlorophyll distributions or sea-surface temperature. However, the transport in the troposphere could be affected by interannual variability in the wind fields rather than, e.g. precipitation fields, with wet deposition of CH_3ONO_2 via precipitation being a minor loss route. Given the weak temperature and pressure dependence of Reaction (10) the chemical production term should also not be influenced, although the differences in background methane mixing ratios of a few tens of ppb will result in a small increase in CH_3ONO_2 via enhanced mixing ratios of CH_3O_2. Moreover, the significant changes in Asian NO_x emissions over the decade which are included in our simulations (Ohara et al., 2007) will not affect such remote regions to any significant extent due to westerly transport away towards the US being dominant (Zhang et al., 2008). The measurement data is binned at a resolution of 100 m altitude in order to aid interpretation of the comparisons. The variability in the measurements can be significant in any one altitude bin (not shown), as measurements used for any particular altitude bin are sampled over a wide range of longitudes as shown in Fig. 6.

Figure 7 shows the comparisons of five different simulations against measured CH_3ONO_2 distributions using data which is sorted between the latitudinal limits of 10–20° N, 10° S–10° N and 10–20° S, respectively. Data taken from both of the aircraft involved in the campaign are aggregated

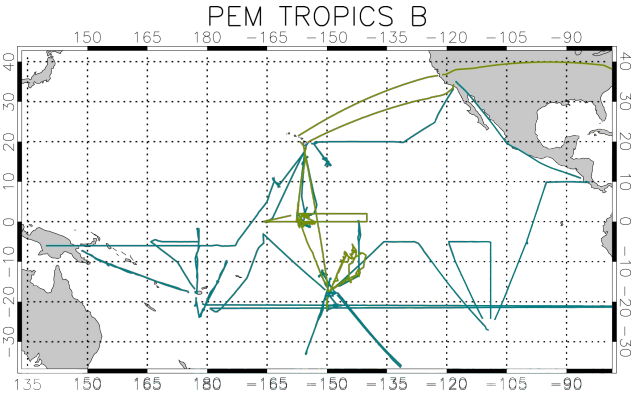

Fig. 6. The flight routes of taken by the DC-8 (cyan) and P-3B (green) during March 1999 as part of the PEM-B Tropics campaign.

and shown on the same comparison, although the number of measurements in each latitudinal bin is not equal, meaning that less weight should be put on the northern comparisons (see Fig. 6). The outputs from EMISS (orange), FLIGHT (light blue) LOWBR (dark blue), FULL (dark red) and DDEP (green) are compared directly. It can be clearly seen from the PEM-B tropics measurements that the vertical distribution in CH_3ONO_2 exhibits the steepest gradient in the tropics between 10° S–10° N, implying a stronger oceanic emission source than the other latitudinal regions, and thus agreeing with the independent observations from ships (Dahl et al., 2005). For the other latitudinal regions the vertical profile is either rather shallow (NH) or appears concave (SH).

The distribution of CH_3ONO_2 in EMISS at 10–20° S and 10–20° N shows the extent of transport out of the tropics during March. Also shown is FLIGHT, which uses double the oceanic emission flux (cf. Table 2). In the NH, EMISS agrees with the observations to a large extent, whereas all the other simulations lead to overestimations of between 5–30 ppt. Thus none of the simulations has the ability to fully capture the correct vertical profile. In the SH, EMISS generally underestimates observed mixing ratios, exhibiting a convex profile in contrast to the observed vertical shape. That there is an underprediction at the surface does imply that direct oceanic emissions could occur south of 10° S. FLIGHT captures the distribution more accurately in the LT and FT, but still has a low bias in the UT. The other simulations, FULL and LOWBR, overestimate near-surface mixing ratios by $\sim$10–15 ppt. As we do not apply either a diurnal or seasonal variation in the emission term, the model cannot be expected to be able to capture exactly the same profile. To improve on this, future studies could exploit chlorophyll maps from satellites such as MODIS as demonstrated by Myriokefalitakis et al. (2010) for marine organic aerosol formation. However, our study is more focussed on the influence of the chemical production term therefore we consider developing such an approach to be beyond the scope of this present study.

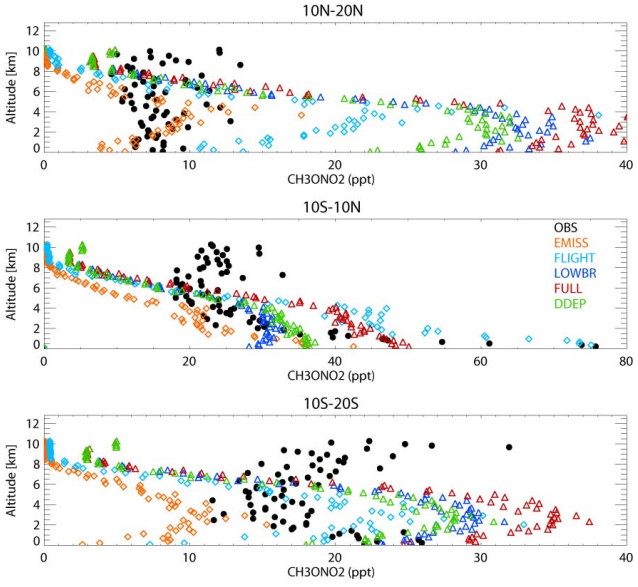

Fig. 7. A comparison of the distribution of CH_3ONO_2 around the tropical Pacific Ocean as measured during March 1999 in the PEM-Tropics B measurement campaign and simulated in TM5. Comparisons are shown for EMISS (orange), FLIGHT (light blue), LOWBR (dark blue), FULL (red) and DDEP (green). The reader should note the different scales on the x axis between latitudinal regions.

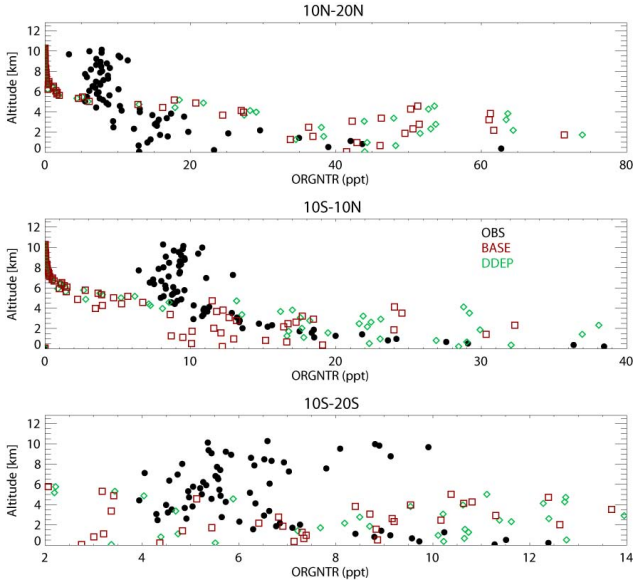

Fig. 8. A comparison of the distribution of higher alkyl nitrates as measured during March in the PEM-Tropics B measurement campaign and that simulated in TM5. The simulations shown are for BASE (blue) and EMISS (orange).

In the tropics EMISS tends to underestimate mixing ratios at the surface, indicating that the emission flux calculated by Neu et al. (2008) is too low. FLIGHT captures the observed mixing ratios rather well at the surface and around 6 km, but overestimates in the LT. The contribution from Reaction (10) is shown in LOWBR, showing the importance of chemical production in the FT and UT, as concluded by Flocke et al. (1998a), albeit at a more efficient rate. Although Reaction (10) improves the comparison in the FT, the persistent low model bias across simulations implies either that photolytic destruction is too fast or there is a missing chemical source term. We comment further on this below when discussing comparisons against the ARCTAS data. Comparing FULL and DDEP shows that the best correlation occurs when emissions, enhanced deposition and chemical production terms, are included in the simulation.

Figure 8 shows the corresponding comparison against the PEM-tropics B data for $RONO_2$ for BASE and DDEP. Here the measurement data represents the sum of different alkyl nitrates, namely $C_2H_5ONO_2$, i-$C_3H_7ONO_2$, n-$C_3H_7ONO_2$ and 2-$C_4H_9ONO_2$. For discussion regarding the chemical production of $RONO_2$ in BASE, the reader is referred to Sect. 4. As for CH_3ONO_2, the introduction of oceanic emissions of $RONO_2$ has little effect away from the source region but improves the quality of the comparison in the tropics between 10° S–10° N, especially at the surface. Again a significant fraction of $RONO_2$ is lost as deposition (see discussion on global chemical budgets in Sect. 3) and there is a persistent low model bias in the UT. Although chemical production mechanisms for $RONO_2$ have been measured involving RO_2 in the laboratory, they are only thought relevant in polluted plumes with elevated mixing ratios of NO_x and VOC (volatile organic carbon) (e.g. Butkovskaya et al., 2010). One additional influence on the lifetime could be that in TM5 the photolysis rate for $RONO_2$ is calculated using the absorption characteristics of 2-$C_4H_9ONO_2$ due to the lack of experimental data for the other higher alkyl nitrates (Williams et al., 2012).

To identify whether the vertical distribution of CH_3ONO_2 is captured better at high northern latitudes away from direct tropical emission sources, Fig. 9 shows comparisons of co-located model output against measurements made during the ARCTAS measurement campaign during April and July 2008 (Jacob et al., 2010). The data is sorted between the latitudinal limits 50–60° N, 60–70° N and > 70° N; most data points exist in the 60–70° N range for April and the 50–60° N range for July due to the shift in where the DC-8 aircraft was based for conducting the observations. For brevity we only show comparisons of those simulations which include Reaction (10), namely FULL (light blue), DDEP (green) and FLIGHT (red).

For both months, the observations show a rather homogeneous vertical profile, similar to that shown above Antarctica in Beyersdorf et al. (2010). Examining the model profiles shows a persist feature across comparisons, with a sharp transition in mixing ratios around 5–6 km, very similar to that which is simulated in the tropics. The comparisons above

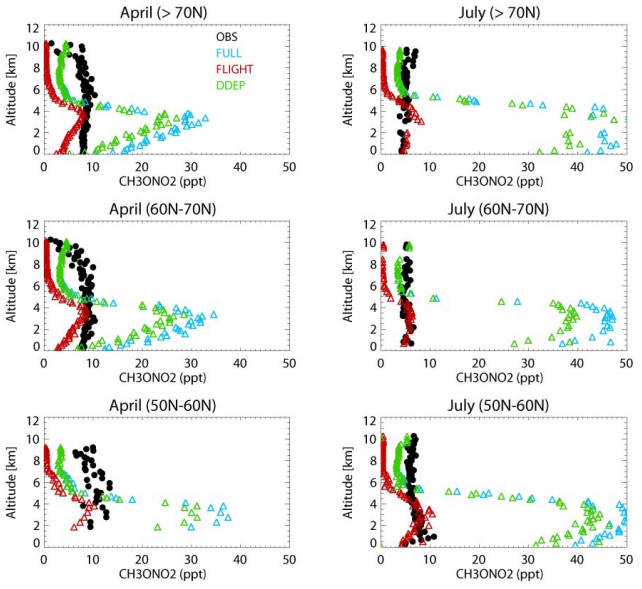

Fig. 9. A comparison of the vertical distribution of CH_3ONO_2 around Alaska (April) and Western Canada (July) as measured during 2008 during the ARCTAS measurement campaign and as simulated in TM5. Comparisons are shown for FULL (light blue), FLIGHT (red) and DDEP (green).

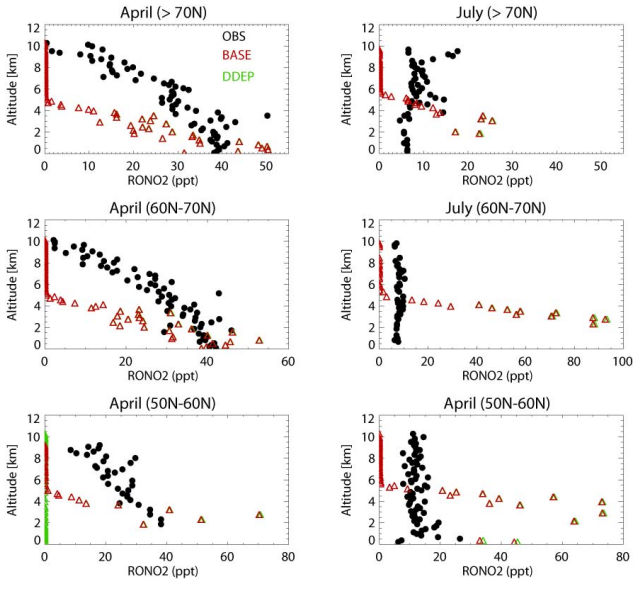

Fig. 10. A comparison of the distribution of higher alkyl nitrates as measured during April and July 2008 during the ARCTAS measurement campaign and simulated by TM5. The simulations shown are for BASE (blue) and EMISS (orange).The reader should note the different scales on the x axis between latitudinal regions.

70° N during April show that there is an overestimation in the FT and an underestimation in the UT, where both photochemical production and destruction are low at this location during April. For FULL and DDEP, overestimations of ∼ 10–20 ppt occur in the LT across all latitude bands, suggesting that there is potentially a missing loss process in TM5, such as heterogeneous scavenging of CH_3O_2 on, e.g. aquated aerosol, as has been postulated for HO_x radical budgets in the Arctic (Mao et al., 2010). That these features also occur in the tropical comparisons (cf. Fig. 7) at similar altitudes for different NO_x environments and at more southerly latitudes, implies that this missing loss process is relevant at a global scale and rules out the influence of weak convective mixing out of the BL. Due to the difference in tropopause height between locations, a stong source of alkyl nitrates from the stratosphere due to downwelling can also be considered to be unimportant in the comparisons. Surprisingly, FLIGHT produces mixing ratios in the LT which agree rather well across the entire measurement domain for both months, although this does not hold for the UT. Comparing profiles between different months shows that the surface mixing ratios simulated in TM5 have a strong seasonal cycle related to the proximity of NO_x sources and photochemical activity, which was not simulated over Antarctica (see Fig. 5 and associated discussion). This is opposite to what is observed in the ARCTAS measurements, where decreases of ∼ 10–20 % occur due to high photochemical destruction during July. This could potentially be due to that the regional soil NO_x emissions are not governed by the meteorological fields used to drive the model, i.e. that the ARCTAS measurements are taken over land which exhibits seasonality in terms of biogenic emissions.

Figure 10 shows the corresponding comparisons for $RONO_2$, where the same higher alkyl nitrates are summed as for the PEM-tropics comparison shown in Fig. 8. The observations show that, in contrast to CH_3ONO_2, there is a decrease in $RONO_2$ with altitude during April, with the profile becoming more homogeneous for July in line with faster photochemical destruction. For the model simulations we only show comparisons for BASE and DDEP, which reveals little difference between the two simulations. The agreement for April is much better than that for July, where a significant overestimation occurs during July similar to that shown for CH_3ONO_2 in Fig. 9. Moreover, another similarity across alkyl nitrates is that TM5 does not capture the measured mixing ratios in the UT for both months, with a sharp transition again occurring around 5–6 km. Table 4 shows that the dominant source of $RONO_2$ in the modified CB05 chemical mechanism involves the XO2N operator species, whose most dominant source is the oxidation of biogenic species. Therefore the discrepancy could be linked to distribution and/or fluxes introduced for these species in the emission inventory. Also the isoprene oxidation scheme included could be considered outdated, considering the latest experimental studies presented in Fuchs et al. (2013). For the UT the comparisons again suggest an unidentified source term.

Finally, Fig. 11 shows comparisons of model output co-located with chemical measurements taken from the

CARIBIC observatory at ∼250 hPa in the northern tropics and subtropics at selected latitudes. We use measurements taken over most of the year during 2008. Although no direct measurements of alkyl nitrates are currently available from CARIBIC due to the measurement technique employed, these measurements allow an assessment of the impact of Reaction (10) on the seasonal variability of NO_y near the tropopause – unlike the other measurements, which are typically limited to a few months of the year. The measurement data is binned using 2° latitudinal intervals, with both the outward and return flight data used for the CARIBIC averages which are shown. The 1-σ deviation from the observed mean is also shown (dashed lines) which quantifies the variability in the measurement data. We compare directly against BASE (orange triangles), FLIGHT (green) and FULL (blue). Examining the seasonal trend in the observations shows that between 15–25° N there is a maximum in NO_y mixing ratios towards the start of the year, which generally decreases by ∼30–50 % towards December. Previous studies have shown that emissions directly below the flight path have an impact on composition of the UT over India (Schuck et al., 2010). This reduction in NO_y through the year may be partially explained by the occurrence of the Indian monsoon, where a larger fraction of NO_y is lost via wet deposition, but also by the change in the location of the tropopause. To a large degree, TM5 manages to capture the seasonal variability in NO_y, although the total NO_y is typically too low across all selected latitudes by ∼10–30 %. It should be noted that the decadel growth in aircraft emissions is not included in the inventory, which would reduce this low bias somewhat. To investigate what fraction of the modelled NO_y is due to total alkyl nitrates, we show comparisons of BASE, where the mixing ratios of CH_3ONO_2 and $RONO_2$ are omitted. It can be seen that they contribute ∼20 % of the total model NO_y, and are therefore less important than either HNO_3 or PAN.

The fractional increase in UT NO_y in FLIGHT is limited to a few percent, even at latitudes nearer the source region. From the PEM-tropics data comparisons shown in Figs. 7 and 8, it can be concluded that the model underestimates CH_3ONO_2 in the UT across the tropics, although the contribution of the missing alkyl nitrates towards the missing NO_y is constrained to less than 100 ppt, and thus is not sufficient to account for the underestimation of NO_y in TM5. Comparing FLIGHT and FULL shows that increasing the branching ratio for Reaction (10) only makes a marginal contribution to the observed seasonal dependence in the UT. For DEMISS and DDEP (not shown) there is little difference from that shown for FLIGHT. One reason for the low bias in the model is the impact of stratospheric intrusions which contain substantial mixing ratios of HNO_3, which the model fails to captures even with the new constraints applied from the ODIN instrument. This can be potentially improved by constraining the stratospheric HNO_3 further down towards the tropopause rather than restricting the application of constraints at 10 hPa. In summary, accounting for the direct emission and chemical formation of alkyl nitrates improves the distribution of NO_y in the UT in TM5.

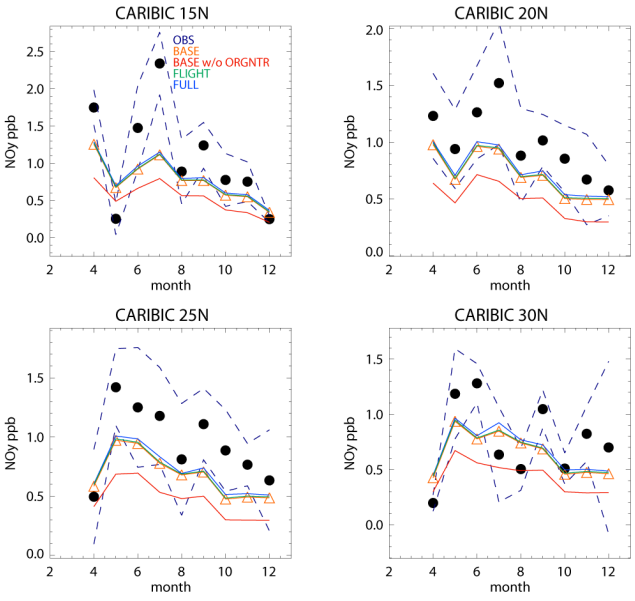

Fig. 11. A comparison of CARIBIC NO_y measurement data (black) sampled in selected latitudinal bins with corresponding model output for the BASE (orange triangles), FLIGHT (green) and FULL (blue). Also shown is BASE NO_y without the contribution from alkyl nitrates (red). The 1-σ variability in the observations is indicated by the dashed blue line.

5 The Impact on global oxidative capacity

Finally in this section we examine the impact of Reaction (10) on the distribution of tropospheric NO_x and O_3, and the subsequent changes in the oxidising capacity of the troposphere via perturbations in OH. In TM5, the transported tracer species NO_x represents the sum of short-lived nitrogen radicals and radical reservoirs, namely NO, NO_2, NO_3, HNO_4 and N_2O_5. Table 5 provides the annual global production efficiency of O_3 by NO_x recycling due to Reactions (1), (2) and (8) for BASE, EMISS, FULL and DDEP, along with deposition totals and the global tropospheric burdens of O_3. In Fig. 12a–c we show the global annual mean distribution of NO_x, O_3 and OH in the LT for BASE, respectively. Also shown are the relative percentage differences between BASE, EMISS and DDEP as integrated in the lower few kilometres of the atmosphere (below ∼800 hPa) for 2008.

Figure 12a shows that the highest annual mean mixing ratios of NO_x occur near regions which have high anthropogenic activity, including visible signatures along shipping tracks. For the remote tropical MBL NO_x mixing ratios are of the order 0–50 ppt, where Browne and Cohen (2012) have shown that alkyl nitrates play an important role towards tropospheric O_3 formation under such chemical regimes. In

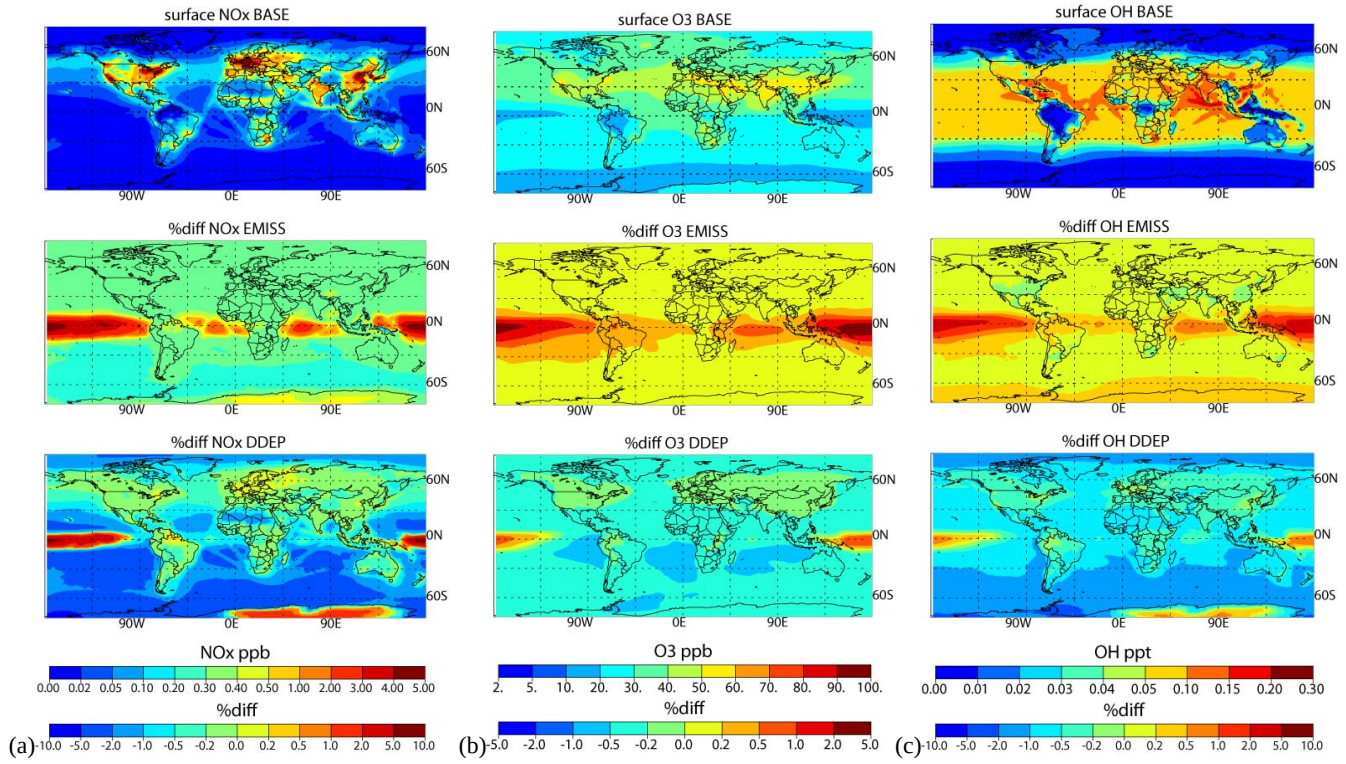

Fig. 12. (a) The annual surface distribution of NO_x integrated below 800hPa (top), along with the percentage differences introduced in the EMISS (middle) and DDEP (bottom) simulations with TM5. The percentage differences are calculated according to (BASE-SENS/BASE)·100. In TM5, NO_x is defined as the sum of NO, NO_2, HNO_4, N_2O_5. **(b)** As in Fig. 10a, except for tropospheric ozone. **(c)** As in Fig. 10a, except for tropospheric OH.

EMISS an increase in NO_x mixing ratios of up to $\sim$10 % occurs around the emission sources in the equatorial Pacific. For other tropical regions, increases are more modest: up to $\pm$2 %. The limited transport and efficient deposition of CH_3ONO_2 in the BL mean that for the subtropics and extratropics effects are limited to around $\pm$0.2 %. Comparing DDEP shows that in the SH there are decreases of around 5–10 %, showing that the transport of NO_x as PAN is reduced by Reaction (10) due to a re-distribution of the amount of nitrogen that exists in the various long-lived reservoir species. That these differences are associated with low values of NO_x means that absolute differences equate to tens of ppt at most.

Figure 12b shows that the largest increases in tropospheric O_3 (of between $\sim$1–5 %) in EMISS are located around the tropics (20° S–20° N) directly near the oceanic sources (see Figs. 1 and 3). Here, O_3 mixing ratios in TM5 are of the order of 20–30 ppb. For the other latitudinal zones there is a more muted increase in tropospheric O_3 associated with the small changes in NO_x (middle panel of Fig. 12a). Table 5 shows that, integrating globally, this equates to a Tg of O_3 (< 0.5 %) in the global tropospheric burden due to an increase in the turnover of Reactions (1) and (2) from the additional NO_x and HO_2 (from enhanced CO oxidation). For DDEP, Reaction (10) suppresses O_3 formation by increasing the fraction of nitrogen lost to the surface and by decreasing the chain length of the NO_x recycling mechanism. Figure 10c shows the associated perturbations in OH in both simulations. A large fraction of chemical oxidation occurs in the tropical BL (Fiore et al., 2006); thus the increases in resident OH have a more marked effect on global atmospheric lifetimes than similar perturbations at higher latitudes. At other latitudes changes in resident OH are in line with the changes in O_3 shown in Fig. 12b. The effect on tropospheric lifetimes is rather small, as shown by the variability shown of both CO and CH_4 in Table 5. In summary, the introduction of Reaction (10) with a branching ratio of 0.3 % completely negates the increase in global oxidative capacity from ocean emissions of alkyl nitrates.

6 Conclusions

In this study we have examined the impact of introducing the direct chemical formation of methyl nitrate (CH_3ONO_2) during NO_x recycling involving the methyl-peroxy radical on the global distribution of CH_3ONO_2, NO_x, O_3 and OH as simulated in a global chemistry transport model. We compare this against the corresponding changes introduced when adopting direct oceanic emission of CH_3ONO_2 and the

Table 5. The annual global chemical budget terms for tropospheric O_3 given in Tg O_3 yr^{-1} for selected simulations.

	BASE	EMISS	FULL	DDEP
$NO + HO_2$	2987.9	2997.9	2981.7	2976.7
$NO + CH_3O_2$	1138.5	1144.2	1132.5	1130.3
$NO + XO_2$	455.6	455.9	455.0	454.9
Total	4582.0	4598.0	4569.3	4562.0
Dry deposition	804.7	806.0	803.19	802.5
Trop. burden	334.3	335.3	334.6	334.1
Trop. CO lifetime (days)	50.94	50.74	51.00	51.09
Trop. CH_4 lifetime (years)	8.42	8.40	8.45	8.47

higher (C2 and above) alkyl nitrates in the tropics (10° S–10° N) as based on a set of independent observations and previous modelling studies.

It is found that the global surface distribution of CH_3ONO_2 is sensitive to the variability in the dry deposition velocity. Analysing the chemical budget reveals that $\sim 50\,\%$ of nitrogen introduced via direct oceanic emission of CH_3ONO_2 is lost by deposition processes close to the source regions, which scales with the emission term. Without direct chemical formation of CH_3ONO_2 we find that the best estimate of the global emission term from the ocean is $\sim 0.57\,Tg\,N\,yr^{-1}$, higher than previous estimates. For higher alkyl nitrates we suggest including an oceanic flux for higher alkyl nitrates equal to $\sim 0.17\,Tg\,N\,yr^{-1}$, approximately double that of previous estimates. Ideally a dedicated future study could impose better constraints of direct oceanic emissions by the derivation of a parameterisation for oceanic emissions related to the distribution of phytoplankton blooms as measured from space and local wind speeds, as has been done for the emission of organics from the ocean.

Using measurements taken at a variety of surface sites, we show that applying the measured branching ratio of 1.0 % for direct chemical formation results in tropospheric mixing ratios of CH_3ONO_2 which are an order of magnitude too high. A previous estimate of the branching ratio (0.025 %) derived from analysing chemical observations in the upper troposphere is also too low to be able to capture observed mixing ratios at the surface. However, adopting a lower limit for the branching ratio of 0.3 % allows the model to capture observed mixing ratios in the Southern Hemisphere without the need of any direct regional oceanic source term, as well as contributing to the observed mixing ratios in the tropics, resulting in a lower emission flux compared to that derived from observations alone. For the Northern Hemisphere, there is a strong seasonal cycle inverse of that which is observed.

For the upper troposphere comparisons, made against a number of different measurement data sets, a persistently significant low model bias exists regardless of the magnitude of the branching ratio or latitude. That this occurs for scenarios with both high and low photochemical activity suggests an as yet unknown missing chemical precursor source or transport pathway. For the upper troposphere in the northern subtropics, the seasonal and latitudinal distribution of NO_y is generally improved when including a mixture of direct emissions and chemical production of CH_3ONO_2, although similar improvements are also simulated when using a high oceanic emission term showing the need for tighter constraints on the strength of the emission source. In general alkyl nitrates account for between 5–10 % of the observed NO_y in the upper troposphere, and are less important than either PAN or HNO_3.

Finally, in terms of tropospheric O_3, the increases which result from the additional nitrogen introduced by the direct emission of alkyl nitrates are essentially reversed on a global scale when accounting for the sequestration of nitrogen due to the chemical formation of CH_3ONO_2.

Based on this study, we recommend that in order to improve the understanding and modelling of alkyl nitrates in the future, three main uncertainties be addressed. Firstly, further laboratory experiments should be performed in order to verify the chemical production of CH_3ONO_2 and provide an independent branching ratio, which can then lead to more concrete recommendations for atmospheric modellers. Secondly, chemical measurements in the remote Northern and Southern Hemispheres above open water should be made to establish whether the direct oceanic flux only exists in the tropics and better constrain the latitudinal variability. Thirdly the deposition of a range of alkyl nitrates should be determined over diverse land types to better constraint the efficiency of physical loss processes.

Acknowledgements. The authors would like to thank L. Emmons (NOAA) for processing the PEM tropics measurement data and providing it for download. We would also like to thank P. le Sager and T. P. C van Noije for implementing bug fixes to the TM5 model.

Edited by: T. Butler

References

Atkinson, R.: Atmospheric chemistry of VOCs and NO_x, Atmos. Environ., 34, 2063–2101, 2000.

Atlas, E., Pollock, W. Greenberg, J., Heidt, L., and Thompson, A. M.: Alkyl nitrates, non-methane hydrocarbons and halocarbon gases over the equatorial Pacific Ocean during Saga 3, J. Geophys. Res., 98, 16933–16947, 1993.

Beyersdorf, A. J., Blake, D. R., Swanson, A., Meinardi, S., Rowland, F. S., and Davis, D: Adundances and variability of tropospheric volatile organic compounds at the South Pole and other Antarctic locations, Atmos. Environ., 44, 4565–4574, 2010.

Blake, N. J., Blake, D. R., Wingenter, O. W., Sive, B. C., Kang, C. H., Thornton, D. C., Bandy, A. R., Atlas, E., Flocke, F., Harris, J. M., and Rowland, F. S.: Aircraft measurements of the latitudinal, vertical and seasonal variations of NMHCs, methyl nitrate, methyl halides, and DMS during the First Aerosol Characteriza-

tion Experiment (ACE 1), J. Geophys. Res., 104, 21803–21817, 1999.

Blake, N. J., Blake, D. R., Swanson, A. L., Atlas, E., Flocke, F., and Rowland, F. S.: Latitudinal, vertical, and seasonal variations of C1-C4 alkyl nitrates in the troposphere over the Pacific Ocean during PEM-Tropics A and B: Oceanic and continental sources, J. Geophys. Res., 108, 8242, doi:10.1029/2001JD001444, 2003a.

Blake, N. J., Blake, D. R., Sive, B. C., Katzenstein, A. S., Meinardi, S., Wingenter, O. W., Atlas, E. L., Flocke, F., Ridley, B. A., and Rowland, F. S.: The seasonal evolution of NMHCs and light alkyl nitrates at middle to high northern latitudes during TOPSE, J. Geophys. Res., 108, 8359, doi:10.1029/2001JD001467, 2003b.

Boxe, C. S., Hamer, P. D., Ford, W., Hoffmann, M., and Shallcross, D. E.: The effect of the novel $HO_2 + NO => HNO_3$ reaction channel at South Pole, Antarctica, Antarctic Sci., 24, 417, doi:10.1017/S0954102012000144, 2012.

Brenninkmeijer, C. A. M., Crutzen, P., Boumard, F., Dauer, T., Dix, B., Ebinghaus, R., Filippi, D., Fischer, H., Franke, H., Frieß, U., Heintzenberg, J., Helleis, F., Hermann, M., Kock, H. H., Koeppel, C., Lelieveld, J., Leuenberger, M., Martinsson, B. G., Miemczyk, S., Moret, H. P., Nguyen, H. N., Nyfeler, P., Oram, D., O'Sullivan, D., Penkett, S., Platt, U., Pupek, M., Ramonet, M., Randa, B., Reichelt, M., Rhee, T. S., Rohwer, J., Rosenfeld, K., Scharffe, D., Schlager, H., Schumann, U., Slemr, F., Sprung, D., Stock, P., Thaler, R., Valentino, F., van Velthoven, P., Waibel, A., Wandel, A., Waschitschek, K., Wiedensohler, A., Xueref-Remy, I., Zahn, A., Zech, U., and Ziereis, H.: Civil Aircraft for the regular investigation of the atmosphere based on an instrumented container: The new CARIBIC system, Atmos. Chem. Phys., 7, 4953–4976, doi:10.5194/acp-7-4953-2007, 2007.

Browne, E. C. and Cohen, R. C.: Effects of biogenic nitrate chemistry on the NO_x lifetime in remote continental regions, Atmos. Chem. Phys., 12, 11917–11932, doi:10.5194/acp-12-11917-2012, 2012.

Buhr, M. P., Parrish, D. P., Norton, R. B., Fehsenfeld, F. C., Sievers, R. E., and Roberts, J. M.: Contribution of organic nitrates to the total reactive nitrogen budget at a rural Eastern US site, J. Geophys. Res., 95, 9809–9816, 1990.

Butkovskaya, N. I., Kukui, A., Pouvesle, N., and Le Bras, G.: Formation of nitric acid in the gas-phase $HO_2 + NO$ reaction: Effects of temperature and water vapour, J. Phys. Chem. A., 109, 6509–6520, doi:10.1021/jp051534v, 2005.

Butkovskaya, N. I., Kukui, A., and Le Bras, G.: HNO_3 forming channel of the $HO_2 + NO$ reaction as a function of pressure and temperature in the ranges of 72–600 Torr and 223–323 K, J. Phys. Chem. A., 111, 9047–9053, 2007.

Butkovskaya, N. I., Rayez, M.-T., Kukui, A., and Le Bras, G.: Water vapor effect on the HNO_3 yield in the $HO_2 + NO$ reaction: experimental and theoretical evidence, J. Phys. Chem. A., 113, 11327–11342, doi:10.1021/jp811428p, 2009.

Butkovskaya, N. I., Kukui, A., and Le Bras, G.: Pressure and temperature dependence of Ethyl Nitrate formation in the $C2H5O_2 + NO$ reaction, J. Phys. Chem. A, 116, 5972–5980, doi:10.1021/jp210710d, 2012.

Cariolle, D., Evans, M. J., Chipperfield, M. P., Butkovskaya, N., Kukui, A., and Le Bras, G.: Impact of the new HNO_3-forming channel of the HO_2+NO reaction on tropospheric HNO_3, NO_x, HO_x and ozone, Atmos. Chem. Phys., 8, 4061–4068, doi:10.5194/acp-8-4061-2008, 2008.

Chuck, A. L., Turner, S. M., and Liss, P. S.: Direct Evidence for a Marine Source of C1 and C2 Alkyl Nitrates, Science, 297, 1151–1154, 2002.

Clemitshaw, K. C., Williams, J., Rattigan, O. V., Shallcross, D. E., Law, K. S., and Cox, R. A.: Gas-phase ultraviolet absorption cross-sections and atmospheric lifetimes of several C2–C5 alkyl nitrates, J. Photochem. Photobiology A, 102, 117–126, 1997.

Dahl, E. E. and Saltzman, E. S.: Alkyl nitrate photochemical production rates in North Pacific seawater, Mar. Chem., 112, 137, doi:10.1016/j.marchem.2008.10.002, 2008.

Dahl, E. E., Yvon-Lewis, S. A., and Saltzman, E. S.: Saturation anomalies of alkyl nitrates in the tropical Pacific Ocean, Geophys. Res. Lett., 32, L20817, doi:10.1029/2005GL023896, 2005.

Dahl, E. E., Yvon-Lewis, S. A., and Saltzman, E. S.: Alkyl nitrate (C1-C3) depth profiles in the tropical Pacific Ocean, J. Geophys. Res., 112, C01012, doi:10.1029/2006JC003471, 2007.

Dee, D. P., Uppala, S. M., Simmons, A. J., Berrisford, P., Poli, P., Kobayashi, S., Andrae, U., Balmaseda, M. A., Balsamo, G., Bauer, P., Bechtold, P., Beljaars, A. C. M., van de Berg, L., Bidlot, J., Bormann, N., Delsol, C., Dragani, R., Fuentes, M., Geer, A. J., Haimberger, L., Healy, S. B., Hersbach, H., Hólm, E. V., Isaksen, L., Kållberg, P., Köhler, M., Matricardi, M., McNally, A. P., Monge-Sanz, B. M., Morcrette, J.-J., Park, B.-K., Peubey, C., de Rosnay, P., Tavolato, C., Thépaut, J.-N., and Vitart, F.: The ERA-Interim reanalysis: configuration and performance of the data assimilation system, Q. J. Roy. Meteorol. Soc., 137, 553–597, 2011.

Farmer, D. K. and Cohen, R. C.: Observations of HNO_3, $\sum$AN, $\sum$PN and NO_2 fluxes: evidence for rapid HO_x chemistry within a pine forest canopy, Atmos. Chem. Phys., 8, 3899–3917, doi:10.5194/acp-8-3899-2008, 2008.

Farmer, D. K., Perring, A. E., Wooldridge, P. J., Blake, D. R., Baker, A., Meinardi, S., Huey, L. G., Tanner, D., Vargas, O., and Cohen, R. C.: Impact of organic nitrates on urban ozone production, Atmos. Chem. Phys., 11, 4085–4094, doi:10.5194/acp-11-4085-2011, 2011.

Fehsenfeld, F. C., Daum, P., Leaitch, W. R., Trainer, M., Parrish, D. D., and Hübler, G., transport and processing of O_3 and O_3 precursors over the North Atlantic: An overview of the 1993 North Atlantic Regional Experiment (NARE) summer intensive, J. Geophys. Res., 101, 28877–28891, 1996.

Fiore, A. M., Horowitz, L. W., Dlugokencky, E. J., and West, J. J.: Impact of meteorology and emissions on methane trends, 1990–2004, Geophys. Res. Lett., 33, L12809, doi:10.1029/2006GL026199, 2006.

Flocke, F., Atlas, E., Madronich, S., Schauffler, S. M., Aikin, K., Margitan, J. J., and Bui, T. P.: Observations of methyl nitrate in the lower stratosphere during STRAT: Implications for gas phase prodcution mechanisms, Geophys. Res. Lett., 25, 1891–1894, 1998a.

Flocke, F., Volz-Thomas, A., Buers, H.-J., Pätz, W., Garthe, H.-J., and Kley, D.: Long-term measurements of alkyl nitrates in southern Germany: 1. General behavior and seasonal and diurnal variation, J. Geophys. Res., 103, 5279–5746, 1998b.

Fuchs, H., Hofzumahaus, A., Rohrer, F., Bohn, B., Brauers, T., Dorn, H.-P., Häseler, R., Holland, F., Kaminski, M., Li, X., Lu, K., Nehr, S., Tillmann, R., Wegener R., and Wahner, A.: Experimental evidence for efficient hydroxyl radical regener-

ation in isoprene oxidation, Nature Geosci., 6, 1023–1026, doi:10.1038/ngeo1964, 2013.

Ganzeveld, L. and Lelieveld, J.: Dry deposition parameterization in a chemistry general circulation model and its influence on the distribution of reactive gases, J. Geophys. Res., 100, 20999–21012, 1995.

Gery, M. W., Whitten, G. Z., Killus, J. P., and Dodge, M. C.: A photochemical kinetics mechanism for urban and regional scale computer modeling, J. Geophys. Res., 94, 925–956, 1989.

Gottschaldt, K., Voigt, C., Jöckel, P., Righi, M., Deckert, R., and Dietmüller, S.: Global sensitivity of aviation NO_x effects to the HNO_3-forming channel of the HO_2 + NO reaction, Atmos. Chem. Phys., 13, 3003–3025, doi:10.5194/acp-13-3003-2013, 2013.

Guenther, A., Karl, T., Harley, P., Wiedinmyer, C., Palmer, P. I., and Geron, C.: Estimates of global terrestrial isoprene emissions using MEGAN (Model of Emissions of Gases and Aerosols from Nature), Atmos. Chem. Phys., 6, 3181–3210, doi:10.5194/acp-6-3181-2006, 2006.

Huijnen, V., Williams, J., van Weele, M., van Noije, T., Krol, M., Dentener, F., Segers, A., Houweling, S., Peters, W., de Laat, J., Boersma, F., Bergamaschi, P., van Velthoven, P., Le Sager, P., Eskes, H., Alkemade, F., Scheele, R., Nédélec, P., and Pätz, H.-W.: The global chemistry transport model TM5: description and evaluation of the tropospheric chemistry version 3.0, Geosci. Model Dev., 3, 445–473, doi:10.5194/gmd-3-445-2010, 2010.

Jacob, D. J., Crawford, J. H., Maring, H., Clarke, A. D., Dibb, J. E., Emmons, L. K., Ferrare, R. A., Hostetler, C. A., Russell, P. B., Singh, H. B., Thompson, A. M., Shaw, G. E., McCauley, E., Pederson, J. R., and Fisher, J. A.: The Arctic Research of the Composition of the Troposphere from Aircraft and Satellites (ARCTAS) mission: design, execution, and first results, Atmos. Chem. Phys., 10, 5191–5212, doi:10.5194/acp-10-5191-2010, 2010.

Jaffe, D., Mahura, A., Kelly, J., Atkins, J., Novelli, P. C., and Merrill, J.: Impact of Asian emissions on the remote North Pacific atmosphere: Interpretation of CO data from Shemya, Guam, Midway and Mauna Loa, J. Geophys. Res., 102, 28627–28635, doi:10.1029/96JD02750, 1997.

Jégou, F., Urban, J., de La Noë, J., Ricaud, P., Le Flochmoën, E., Murtagh, D. P., Eriksson, P., Jones, A., Petelina, S., Llewellyn, E. J., Lloyd, N. D., Haley, C., Lumpe, J., Randall, C., Bevilacqua, R. M., Catoire, V., Huret, N., Berthet, G., Renard, J. B., Strong, K., Davies, J., Mc Elroy, C. T., Goutail, F., and Pommereau, J. P.: Technical Note: Validation of Odin/SMR limb observations of ozone, comparisons with OSIRIS, POAM III, ground-based and balloon-borne instruments, Atmos. Chem. Phys., 8, 3385–3409, doi:10.5194/acp-8-3385-2008, 2008.

Jones, A. E., Wolff, E. W., Ames, D., Bauguitte, S. J.-B., Clemitshaw, K. C., Fleming, Z., Mills, G. P., Saiz-Lopez, A., Salmon, R. A., Sturges, W. T., and Worton, D. R.: The multi-seasonal NO_y budget in coastal Antarctica and its link with surface snow and ice core nitrate: results from the CHABLIS campaign, Atmos. Chem. Phys., 11, 9271–9285, doi:10.5194/acp-11-9271-2011, 2011.

Kames, J. and Schurath, U.: Alkyl nitrates and bifunctional nitrates of atmospheric interest: Henry's law constants and their temperature dependencies, J. Atmos. Chem., 15, 79–95, 1992.

Mao, J., Jacob, D. J., Evans, M. J., Olson, J. R., Ren, X., Brune, W. H., Clair, J. M. St., Crounse, J. D., Spencer, K. M., Beaver, M. R., Wennberg, P. O., Cubison, M. J., Jimenez, J. L., Fried, A., Weibring, P., Walega, J. G., Hall, S. R., Weinheimer, A. J., Cohen, R. C., Chen, G., Crawford, J. H., McNaughton, C., Clarke, A. D., Jaeglé, L., Fisher, J. A., Yantosca, R. M., Le Sager, P., and Carouge, C.: Chemistry of hydrogen oxide radicals (HO_x) in the Arctic troposphere in spring, Atmos. Chem. Phys., 10, 5823–5838, doi:10.5194/acp-10-5823-2010, 2010.

Meijer, E. W., van Velthoven, P. F. J., Brunner, D. W., Huntrieser, H., and Kelder, H.: Improvement and evaluation of the parameterisation of nitrogen oxide production by lightning, Phys. Chem. Earth, 26, 557–583, 2001.

Myriokefalitakis, S., Vignati, E., Tsigaridis, K., Papadimas, C., Sciare, J., Mihalopoulos, N., Facchini, M. C., Rinaldi, M., Dentener, F. J., Ceburnis, D., Hatzianastasiou, N., O'Dowd, C. D., van Weele, M. and Kanakidou, M.: Global Modeling of the Oceanic Source of Organic Aerosols, Adv. Meteorol., 2010, 939171, doi:10.115/2010/939171, 2010.

Neu, J. L., Lawler, M. J., Prather, M. J., and Saltzman, E. S.: Oceanic alkyl nitrates as a natural source of tropospheric ozone, Geophys. Res. Lett., 35, L13814, doi:10.1029/2008GL034189, 2008.

Ohara, T., Akimoto, H., Kurokawa, J., Horii, N., Yamaji, K., Yan, X., and Hayasaka, T.: An Asian emission inventory of anthropogenic emission sources for the period 1980–2020, Atmos. Chem. Phys., 7, 4419–4444, doi:10.5194/acp-7-4419-2007, 2007.

Orlando, J. J., Tyndall, G. S., and Calvert, J. G.: Thermal decomposition pathways for peroxyacetyl nitrate (PAN): Implications for atmospheric methyl nitrate levels, Atmos. Environ., 26A, 3111–3118, 1992.

Perrier, S., Houdier, S., Dominé, F., Cabanes, A., Legagneux, L., Sumner, A. L., and Shepson, P. B.: Formaldehyde in Arctic snow. Incorporation into ice particles and evolution in the snowpack, Atmos. Environ., 36, 2695–2705, 2002.

Raper, J. L., Kleb, M. M., Jacob, D. J., Davis, D. D., Newell, R. E., Fuelberg, H. E., Bendura, R. J., Hoell, J. M., and McNeal, R. J.: Pacific Exploratory Mission in the Tropical Pacific: PEM-Tropics B, March–April 1999, J. Geophys. Res., 106, 32401–32425, doi:10.1029/2000JD900833, 2001.

Reeves, C. E., Slemr, J., Oram, D. E., Worton, D., Penkett, S. A., Stewart, D. J., Purvis, R., Watson, N., Hopkins, J., Lewis, A., Methven, J., Blake, D. R., and Atlas, E.: Alykl nitrates in outflow from North America over the North Atlantic during Intercontinental Transport of Ozone and Precursors 2004, J. Geophys. Res., 112, D10, doi:10.1029/2006JD007567, 2007.

Ridley, B. A. and Robinson, E.: The Mauna Loa Observatory Photochemical Experiment, J. Geophys. Res., 97, 10285–10290, 1992.

Roberts, J. M., Bertman, S. B., Parrish, D. D., Fehsenfeld, F. C., Jobson, B. T., and Niki, H.: measurement of alkyl nitrates at Chebogue Point, Nova Scotia during the 1993 North Atlantic Regional Experiment (NARE) intensive, J. Geophys. Res., 103, 13569–13580, 1998.

Russo, R. S., Zhou, Y., Haase, K. B., Wingenter, O. W., Frinak, E. K., Mao, H., Talbot, R. W., and Sive, B. C.: Temporal variability, sources, and sinks of C1–C5 alkyl nitrates in coastal New England, Atmos. Chem. Phys., 10, 1865–1883, doi:10.5194/acp-10-1865-2010, 2010.

Sander, R.: Compilation of Henry's Law Constants for Inorganic and Organic Species of Potential Importance in Environ-

mental Chemistry, Mainz, Germany, available at: http://www.mpch-mainz.mpg.de/~sander/res/henry.html, 1999.

Sander, S. P., Abbatt, J. R., Burkholder, J. B., Friedl, R. R., Golden, D. M., Huie, R. E., Kolb, C. E., Kurylo, M. J., Moortgat, G. K., Orkin, V. L., and Wine, P. H.: Chemical kinetics and Photochemical Data for Use in Atmospheric studies, Evaluation No.17, JPL Publication 10-6, Jet Propulsion Laboratory, Pasadena, available at: http://jpldataeval.jpl.nasa.gov, 2011.

Sanderson, M. G., Collins, W. J., Derwent, R. G., and Johnson, C. E.: Simulation of global hydrogen levels Uusing a Lagrangian Three-Dimensional Model, J. Atmos. Chem., 46, 15–48, 2003.

Schuck, T. J., Brenninkmeijer, C. A. M., Baker, A. K., Slemr, F., von Velthoven, P. F. J., and Zahn, A.: Greenhouse gas relationships in the Indian summer monsoon plume measured by the CARIBIC passenger aircraft, Atmos. Chem. Phys., 10, 3965–3984, doi:10.5194/acp-10-3965-2010, 2010.

Schultz, M. G., Backman, L., Balkanski, Y., Bjoerndalsaeter, S., Brand, R., Burrows, J. P., Dalsøeren, S., de Vasconcelos, M., Grodtmann, B., Hauglustaine, D. A., Heil, A., Hoelzemann, J. J., Isaksen, I. S. A., Kaurola, J., Knorr, W., Ladstaetter-Weissenmayer, A., Mota, B., Oom, D., Pacyna, J., Panasiuk, D., Pereira, J. M. C., Pulles, T., Pyle, J., Rast, S., Richter, A., Savage, N., Schnadt, C., Schultz, M., Spessa, A., Staehelin, J., Sundet, J. K., Szopa, S., Thonicke, K., van het Bolscher, M., van Noije, T. van Velthoven, P. Vik, A. F., and Wittrock, F.: REanalysis of the TROpospheric chemical composition over the past 40 years (RETRO) – A long-term global modeling study of tropospheric chemistry, Final Report, Jülich/Hamburg, Germany, 2007 (Published as report no. 48/2007 in the series "Reports on Earth System Science" of the Max Planck Institute for Meteorology, Hamburg, ISSN 1614-1199), 2007.

Simpson, I. J., Meinardi, S., Blake, D. R., Blake, N. J., Rowland, F. S., Atlas, E., and Flocke, F.: A biomass burning source of C1–C4 alkyl nitrates, Geophys. Res. Lett., 29, 2168, doi:10.1029/2002GL016290, 2002.

Søvde, O. A., Hoyle, C. R., Myhre, G., and Isaksen, I. S. A.: The HNO_3 forming branch of the HO_2 + NO reaction: pre-industrial-to-present trends in atmospheric species and radiative forcings, Atmos. Chem. Phys., 11, 8929–8943, doi:10.5194/acp-11-8929-2011, 2011.

Spahni, R., Wania, R., Neef, L., van Weele, M., Pison, I., Bousquet, P., Frankenberg, C., Foster, P. N., Joos, F., Prentice, I. C., and van Velthoven, P.: Constraining global methane emissions and uptake by ecosystems, Biogeosciences, 8, 1643–1665, doi:10.5194/bg-8-1643-2011, 2011.

Stevenson, D. S., Dentener, F. J., Schultz, M. G., Ellington, K., van Noije, T. P. C., Wild, O., Zeng, G., Amann, M., Atherton, C. S., Bell, N., Bergmann, D. J., Bey, I., Butler, T., Cofala, J., Collins, W.J., Derwent, R. G., Doherty, R. M., Brevet, J., Eskes, H. J., Fiore, A. M., Gauss, M., Hauglustaine, D. A., Horowitz, L. W., Isaksen, I. S. A., Krol, M. C., Lamarque, J.-F., Lawrence, M. G., Montanaro, V., Müller, J.-F., Pitari, G., Prather, M. J., Pyle, J. A., Rast, S., Rodriguez, J. M., Sanderson, M. G., Savage, N. H., Shindell, D. T., Strahan, S. E., Sudo, K., and Szopa, S.: Multimodel ensemble simulations of present-day and near-future tropospheric ozone, J. Geophys. Res., 111, D08301, doi:10.1029/2005JD006338, 2006.

Swanson, A. L., Blake, N. J., Atlas, E., Flocke, F., Blake, D. R., and Rowland, F. S.: Seasonal variations of C2–C4 non-methane hydrocarbons and C1–C4 alkyl nitrates at the Summit research station in Greenland, J. Geophys. Res., 108, 4065, doi:10.1029/2001JD001445, 2003.

Swanson, A. L., Davis, D. D., Arimoto, R., Roberts, P., Atlas, E.L., Flocke, F., Meinardi, S., Rowland, F. S., and Blake, D. R.,Organic trace gases of oceanic origin observed at South Pole during ISCAT 2000, Atmos. Environ., 38, 5463–5472, 2004.

Talukdar, R. K., Herndon, S. C., Burkholder, J. B., Roberts, J. M., and Ravishankara, A. R.: Atmospheric fate of several alkyl nitrates, part 1:Rate coefficients of the reactions of alkyl nitrates with isotopically labelled hydroxyl radicals, J. Chem. Soc. Faraday Trans., 93, 2787–2796, 1997a.

Talukdar, R. K., Burkholder, J. B., Hunter, M., Gilles, M. K., Roberts, J. M., and Ravishankara, A. R.: Atmospheric fate of several alkyl nitrates, part 2: UV absorption cross-sections and photodissociation quantum yields, J. Chem. Soc. Faraday Trans., 93, 2797–2805, 1997b.

Thomas, J. L., Dibb, J. E., Huey, L. G., Liao, J., Tanner, D., Lefer, B., von Glasow, R., and Stutz, J.: Modeling chemistry in and above snow at Summit, Greenland – Part 2: Impact of snowpack chemistry on the oxidation capacity of the boundary layer, Atmos. Chem. Phys., 12, 6537–6554, doi:10.5194/acp-12-6537-2012, 2012.

Urban, J., Pommier, M., Murtagh, D. P., Santee, M. L., and Orsolini, Y. J.: Nitric acid in the stratosphere based on Odin observations from 2001 to 2009 – Part 1: A global climatology, Atmos. Chem. Phys., 9, 7031–7044, doi:10.5194/acp-9-7031-2009, 2009.

van der A, R. J., Allaart, M. A. F., and Eskes, H. J.: Multi sensor reanalysis of total ozone, Atmos. Chem. Phys., 10, 11277–11294, doi:10.5194/acp-10-11277-2010, 2010.

van der Werf, G. R., Randerson, J. T., Giglio, L., Collatz, G. J., Mu, M., Kasibhatla, P. S., Morton, D. C., DeFries, R. S., Jin, Y., and van Leeuwen, T. T.: Global fire emissions and the contribution of deforestation, savanna, forest, agriculture, and peat fires (1997–2009) Atmos. Chem. Phys., 10, 11707–11735, 2010, http://www.atmos-chem-phys.net/10/11707/2010/.

Walega, J. G., Ridley, B. A., Madronich, S., Grahek, F. E., Shetter, D., Sauvain, T. D., Hahn, C. J., Merill, J. T., Bodhaine, B. A., and Robinson, E.: Observations of peroxyacetyl nitrate, peroxypropionyl nitrate, methyl nitrate and ozone during the Mauna Loa Observatory Photochemical Experiment, J. Geophys. Res., 97, 10311–10330, 1992.

Wang, Y., Choi, Y., Zeng, T., Davis, D., Buhr, Martin, Huey, L. G., and Neff, W.: Assessing the photochemical impact of snow NO_x emissions over Anarctica during ANTCI 2003, Atmos. Environ., 41, 3944–3958, 2007.

Weller, R., Jones, A. E., Wille, A., Jacobi, H.-W., McIntyre, H. P., Sturges, W. T., Huke, M., and Wahenbach, D.: Seasonality of reactive nitrogen oxides (NO_y) at Neumayer Station, Antarctica, J. Geophys. Res., 107, 4673, doi:10.1029/2002JD002495, 2002.

Williams, J. E., van Velthoven, P. F. J., and Brenninkmeijer, C. A. M.: Quantifying the uncertainty in simulating global tropospheric composition due to the variability in global emission estimates of Biogenic Volatile Organic Compounds, Atmos. Chem. Phys., 13, 2857–2891, doi:10.5194/acp-13-2857-2013, 2013.

Yarwood, G., Rao, S., Yocke, M., and Whitten, G.: Updates to the carbon bond chemical mechanism: CB05. Final report to the US EPA, EPA Report Number: RT-0400675, available at: www.camx.com (last access: November 2013), 2005.

Yonemura, S., Kawashima, S., and Tsuruta, H.: Carbon monoxide, hydrogen and methane uptake by soils in a temperate arable field and a forest, J. Geophys. Res.-Atmos., 105, 14347–14362, 2000.

Zhang, L., Jacob, D. J., Boersma, K. F., Jaffe, D. A., Olson, J. R., Bowman, K. W., Worden, J. R., Thompson, A. M., Avery, M. A., Cohen, R. C., Dibb, J. E., Flock, F. M., Fuelberg, H. E., Huey, L. G., McMillan, W. W., Singh, H. B., and Weinheimer, A. J.: Transpacific transport of ozone pollution and the effect of recent Asian emission increases on air quality in North America: an integrated analysis using satellite, aircraft, ozonesonde, and surface observations, Atmos. Chem. Phys., 8, 6117–6136, doi:10.5194/acp-8-6117-2008, 2008.